CHALMERS

A Method to Estimate Material Data of Rubber Compounds with the Aid of Finite-Element Models

Maters's Thesis in the Master's Programme in Sound and Vibration

JONAS SVENSSON

Department of Civil and Environmental Engineering
Division of Applied Acoustics
Vibroacoustics Group
CHALMERS UNIVERSITY OF TECHNOLOGY
Göteborg, Sweden
Master's Thesis 2006:11

MASTER'S THESIS 2006:11

A Method to Estimate Material Data for Rubber Compounds With the Aid of Finite-Element Models

Master's thesis in the Master's programme in Sound and Vibration

Jonas Svensson

Department of Civil and Environmental Engineering
Division of Applied Acoustics, Vibroacoustic Group
Chalmers University of Technology
Göteborg, Sweden, 2006

A Method to Estimate Material Data for Rubber Compounds with the Aid of Finite-Element Models
Master's thesis in the Master's programme in Sound and Vibration
JONAS SVENSSON

Master's Thesis 2006:11
Department of Civil and Environmental Engineering
Division of Applied Acoustics
Vibroacoustic Group
Chalmers University of Technology
SE-412 96 Göteborg, Sweden
Telephone + 46 (0) 31-772 1000

Printed by
Chalmers Reproservice
Göteborg, Sweden, 2006

A Method to Estimate Material Data for Rubber Compounds
with the Aid of Finite-Element Models.
Master's Thesis in the Master's programme in Sound and Vibration
JONAS SVENSSON
Department of Civil and Environmental Engineering
Division of Applied Acoustics
Vibroacoustics Group
Chalmers University of Technology

Abstract

To have reliable experimental data when forming mathematical models has always been an important aspect within numerous fields of engineering. Specifically, working with models concerning the contact between road surface and tyre, it is vital to have knowledge of the mechanical properties of the rubber compound in the tyre. Values given in tables may not always be completely accurate. The aim of this thesis is to present and evaluate a method of investigating dynamical material properties of rubber compounds, i.e. viscoelastic materials.

The fundamental principle of this method is a velocity profile comparison. The response of a sinusoidally excited, beam-like rubber sample is measured along the sample with a laser Doppler vibrometer. A velocity profile is interpolated from the solution of a finite-element model. The error that arises from the comparison is minimized using a gradient descent algorithm that continuously updates the material data the finite-element model.

The method proposed successfully determines stiffness and damping over a broad frequency range. Results depict good agreement of the velocity profiles, and independent measurements indicate repeatability of the method. The limits of the methods seems to be governed by measurement accuracy.

Keywords: Tire tread material, viscoelasticity, finite-element modeling, error optimization, model updating.

En metod för att uppskatta materialparametrar i gummimaterial-
med hjälp av finita element-modeller.
Examensarbete inom civilingengörsprogrammet Väg och Vattenbyggnad
JONAS SVENSSON
Instutionen för Bygg- och Miljöteknik
Avdelnigen för Teknisk Akustik
Vibroakustiska gruppen
Chalmers tekniska högskola

Sammanfattning

Att ha pålitlig material data när man ställer upp och löser matematiska modeller har alltid varit en viktig del inom flertalet ingenjörområden, så också inom vibrationsakustik. Arbete med modeller som berör kontakten mellan däck och vägyta kräver kunskap om däcksgummits dynamiska egenskaper. Målet med detta examensarbete är därför att presentera och utvärdera en metod för att undersöka dynamiska egenskaper av däcksgummimaterial, det vill säga viskoelastiska material.

Metodens grundläggande princip är en hastighetsprofilsjämförelse mellan mätning och numerisk modellering. Responsen av ett sinusexiterad, balkliknande gummiprov mäts utmed provet med en laser Doppler vibrometer. En hastighetsprofil interpoleras fram från lösningen av en finit element-model. Felet mellan hastighetsprofilerna minimeras av en gradient algorithm som updaterar materialparametrarna i finita element-modellen.

Den presenterade modellen uppskattar framgånsrikt styvhet och dämpning över ett brett frekvensområde. Hastighetsprofilerna visar god överensstämmelse och oberoende mätdata visar på repeterbarhet hos metoden. Mätnogranheten är den huvudsakliga begränsande faktorn hos metoden.

Nyckelord: Däcksgummimaterial, viskoelasticitet, finit element-modellering, optimerings algoritmer, modelluppdatering.

Preface

This Masters Thesis is written at the division of Applied Acoustics (Teknisk Akustik) at Chalmers Universtity of Technology under supervision of Ph.D. Patrik Andersson. This thesis is for the degree of Master of Science (Civilingenjör).

Acknowledgements

A great thanks goes to my supervisor/mentor at the division of Applied Acoustics, Patrik Andersson for always having his door open to any kind of questions I had.

Thanks goes to Börje Wiik at the division of Applied Acoustics for helping with computer- and measurements equipment issues.

Thanks to all the other people at the division of Applied Acoustics who in some way contributed by answering question or helping out with equipment.

Finally I want to thank my family for all the support and comfort during my four and a half years as a student at Chalmers.

Contents

Abstract iii

Sammanfattning iv

1 Introduction 1
- 1.1 Purpose and background . . . 1
- 1.2 Limitations . . . 2
- 1.3 Structure . . . 2
- 1.4 Notation . . . 3

2 Polymer-elostomers 7
- 2.1 Viscoelasticity . . . 7
- 2.2 Chemical composition of treads . . . 10
- 2.3 Frequency-thermal zones of rubber . . . 11

3 Traditional methods for determining material properties 13
- 3.1 Static testing . . . 13
- 3.2 Dynamic testing . . . 15
- 3.3 ISO standards . . . 15
- 3.4 Limitations of traditional methods . . . 17

4 Velocity profile matching method 19
- 4.1 Physical principles of the method . . . 19
- 4.2 Modeling . . . 20
  - 4.2.1 Finite Element Method . . . 20
  - 4.2.2 Wave model . . . 24
- 4.3 Measurements . . . 25
  - 4.3.1 Sample preparation . . . 25
  - 4.3.2 Setup . . . 27
  - 4.3.3 Measuring boundary conditions . . . 29
  - 4.3.4 Limitations . . . 29
  - 4.3.5 Primary evaluation of measurement results . . . 31
- 4.4 Algorithms for updating material parameters . . . 32

4.4.1 Object function 32
4.4.2 Descent algorithms 32
4.4.3 Grid searches 34
4.5 Primary work 35

5 Results **39**
5.1 Dynamic modulus and loss factor 39
5.2 Scatter 44
5.3 Discussion 45

6 Conclusions **47**

A FEM applied to structural mechanics **49**

B Theory of Laser Doppler Vibrometer (LDV) **53**
B.1 Fundamental physics of the LDV 53
B.2 Averaging 54

C Velocity profiles **55**
C.1 Sample set: 1 55
C.2 Sample set: 2 58
C.3 Sample set: reduced sample C 60

D Measurement equipment **63**

References **65**

Chapter 1
Introduction

The introduction chapter gives a brief background to the purpose and the problems behind this thesis. It also provides a short summary of the chapters included.

1.1 Purpose and background

To enable computation of mathematical models, input data is required in order for the models to produce meaningful output. When working with e.g. tyre/road contact models it is the rubber tread in the tyre which is the material in question. Therefore it lies a great interest in having reliable testing methods that reveals the properties of the material. Numerous different methods and testing equipment have been used during the years in order to obtain this information, but still no method has proven to be superior in a wide frequency range.

The purpose of this thesis is to investigate and evaluate a method of accumulating material properties out of rubber tread materials. The material parameters that is being estimated are dynamic stiffness and damping. The method is based on a velocity profile comparison between results from a numerical model and measurements. The rubber tread is cut into beam shaped samples. The samples are submitted to sinusoidal excitation by a mechanical shaker. The response is measured along the center line of the sample with a laser Doppler vibrometer. This provides a measured velocity profile and also information used for input data in the numerical model. The model is a finite-element model consisting of a block of solid elements. A velocity profile is then interpolated from the node values of the finite-element solution. This is being compared with the measured velocity profile and the squared error between them is calculated. The error is then used as the object function for a descent algorithm optimization. More specifically, the material parameter values in the finite-element model are updated and a new error is computed. This process is repeated until the error converges to a minimum value. The procedure is conducted at discrete frequencies between 500 Hz and 5000 Hz. This method is in this thesis referred to as the "velocity profile matching method" (VPMM).

1.2 Limitations

The thesis aims at determining dynamic stiffness and damping in the form of a Young's modulus and a loss factor, for tyre tread materials. The goal is to give values within circa a 10% interval. Testing is conducted within the frequency range between 500 Hz and 5000 Hz. The particular frequency range is chosen in order to cover a wide frequency range that is of interest for tyre/road noise research. The higher end of the frequency range is expected to possibly reveal the frequency limitation of the method.

The thesis focuses on presenting the method and show results for single samples, it does not claim to present results that show full statistical significance. Although measurement and simulations are carried out more than once to test repeatability.

1.3 Structure

The thesis is structured as following;

- *Chapter 2* considers the tread material investigated by the presented method. The chemical composition of rubber compounds and how it behaves under various conditions, e.g frquency and/or temperature changes, are give. The concept of viscoelasticity is described.

- *Chapter 3* provides an overview of some existing methods of determining material properties of viscoelatstic materials. A brief description of how they work, what kind of information is gained from them and why there still is of great interest to investigate new methods, is given.

- In *chapter 4* the velocity profile matching method is presented. The fundamental physical principles, how data is collected and evaluated and limitations for the method. The numerical model behind calculations and the process for updating the material parameters in this model, is explained. The measurements that were conducted in order to gather data, are presented.

- In *chapter 5* the material properties revealed by the method is presented. Also some typical velocity profiles are presented. The results are discussed briefly.

- *Chapter 6* provides the finial conclusions reached after completion of this thesis. Also possible future work that might improve the method is mentioned.

The appendix includes some additional information that may be of interest to the reader. In the main body excessively detailed theory, behind the finite-element method, is avoided. Mathematical derivations that might be of concern for the inclined reader can be found in *Appendix A*. Some information about the Laser

Doppler Vibrometer, used for the measurements, is included in *Appendix B*. Additional results not included in results section is inserted in *Appendix C*. These results contain velocity profiles for all the tested frequencies. *Appendix D* reveals which type of equipment was used to conduced the measurements.

1.4 Notation

Abbreviations

FEM	Finite Element Method
LDV	Laser Doppler Vibrometer
VPMM	Velocity Profile Matching Method
e.g.	exempli gratia
etc.	et cetera
i.e.	id est

Roman upper case letters

B	Bending stiffness	$[m^2 \cdot N]$
$\mathbf{C}$	Damping matrix	$[N \cdot m^{-2}]$
$\mathbf{D}$	Consitutive matrix	$[Pa]$
E	Young's modulus	$[Pa]$
F	Force	$[N]$
G	Shear modulus	$[Pa]$
$\mathbf{K}$	Stiffness matrix	$[Pa]$
M	Moment	$[Nm]$
$\mathbf{M}$	Mass matrix	$[Kg]$
$\mathbf{R}$	External force matrix	$[N]$
U	Volume force	$[N]$
W	Object function weight	[-]

Roman lower case letters

c	Damping coefficients	$[s]$,$[s^2]$
e	Natural logarithm base	[-]
f	Frequency	$[Hz]$
h	Search direction	[-]
j	Imaginary unit $\sqrt{-1}$	[-]
k	Wave number	$[rad \cdot m^{-1}]$
p	Material parameters	$[Pa]$,[-]
u	Displacement	$[m]$

t	Time	$[s]$
v	Velocity	$[m \cdot s^{-1}]$
v	Weak formulation weight function	[-]
x	Distance	$[m]$
z	Error	[-]

Greek letters

α	Step size	[-]
β	Bending angle	$[rad]$
γ	Momentum term factor	[-]
γ	Shear strain	[-]
δ	Phase shift	$[rad]$
ε	Extensional strain	[-]
η	Loss factor	[-]
λ	Wavelength	$[m]$
ν	Poisson's ratio	[-]
π	3.141592...	[-]
ρ	Density	$[kg \cdot m^{-3}]$
ξ	Normal displacement	$[m]$
σ	Extensional stress	$[Pa]$
τ	Shear stress	$[Pa]$
ψ	Shape function	[-]
ω	Angular frequency	$[rad \cdot s^{-1}]$

Subscripts and superscripts

+	Positively traveling
-	Negatively traveling
j	Near field
Calc	Calculated
Meas	Measured
app	Approximate

Various symbols

$\Re[\dots]$	Real part of argument
$\Im[\dots]$	Imaginary part of argument
$\underline{X}$	Denotes X as a complex number
$\mathbf{X}$	Denotes X as a vector or a matrix
$\hat{X}$	Denotes the amplitude of X

X'	Storage modulus of complex modulus X
X''	Loss modulus og complex modulus X
X^T	Transpose of X
$\dot{X}$	Time derivative of X

Chapter 2

Polymer-elostomers

The material used in tyre treads can be a composite of various types of rubber. Rubber is an elastomer belonging to the polymers. These types of materials show a viscoelastic behavior, meaning they have booth viscous (dissipation of energy) and elastic (storage of energy) properties. The elastic and viscous behavior of the polymer is not constant, varying significantly e.g. with frequency and temperature.

2.1 Viscoelasticity

Polymers are materials composed of long intertwined and cross-linked molecular chains. The internal interaction between the molecules cause the material to have certain stiffness and damping properties. A rubber tread is a viscoelastic material, meaning that it shows both elastic and viscous behavior. Elastic means that the vibrational energy is stored in the material while viscous means that it is dissipated (normally in the form of heat). These properties vary with temperature and frequency but it is linear, within certain limits, with respect to vibration amplitude (Jones 2001). However, it is not stated that the material properties are constant with respect to large strain amplitudes. For example polymer used for vibration damping underneath heavy machinery, where the strain is constantly high, the material can not be assumed linear with respect to vibration amplitudes. If the material is homogenous and isotropic, its viscoelastic properties are independent of where in the material your are looking or in which direction the material is loaded.

It is very convenient to work in the frequency domain with mechanical vibrations of viscoelastic materials. Because the time history of the stress and strain in the material are harmonic with a time lag between them (see Figure 2.1). If sinusoidal excitation is assumed it is possible to express the strain and the stress with an amplitude and a phase. The phase shift between the stress and the strain can take an arbitrary number between 0 and $\frac{\pi}{2}$, depending on the viscoelastic properties of the material. The more viscous the material is the bigger the phase shift becomes. The phase shifted strain can be composed of two part, one part in phase with the stress and one part $\frac{\pi}{2}$ out of phase with the stress (see Figure 2.2). The phase lag

can mathematically be expressed by using complex notation when defining the stress-strain (constitutive) relation according to,

$$\underline{\sigma} = \underline{E}\underline{\varepsilon}. \tag{2.1}$$

This relation is known as Hooke's law, and $\underline{E}$ represents a material dependent term referred to as Young's modulus or modulus of elasticity and is defined as,

$$\underline{E} = E' + jE'' \tag{2.2}$$

To get the physical quantity stress, the real part is extracted of equation (2.1) according to,

$$\Re[\underline{\sigma}] = \Re[\underline{\varepsilon E}] = \Re[(E' + jE'')(\hat{\varepsilon}e^{-j\omega t})] = \hat{\varepsilon}(E'cos(\omega t) + E''sin(\omega t)) \tag{2.3}$$

Following the prior reasoning of having two strain portions, one in phase and one out of phase with the stress, it is clear that the amplitudes (E' and E'') determines the phase shift between stress and strain. Hence, the phase lag between stress and strain is modeled by the complex modulus. The real and imaginary part of the complex modulus are referred to as storage modulus (E') and loss modulus (E''). Sometimes it is of interest to give the ratio between storage- and loss modulus, this is referred to as the loss factor (η), and is defined as,

$$\eta \equiv \frac{\Im[\underline{E}]}{\Re[\underline{E}]} = \frac{E''}{E'}. \tag{2.4}$$

Using the loss factor notation the complex modulus can be written as,

$$\underline{E} = E'(1 + j\eta). \tag{2.5}$$

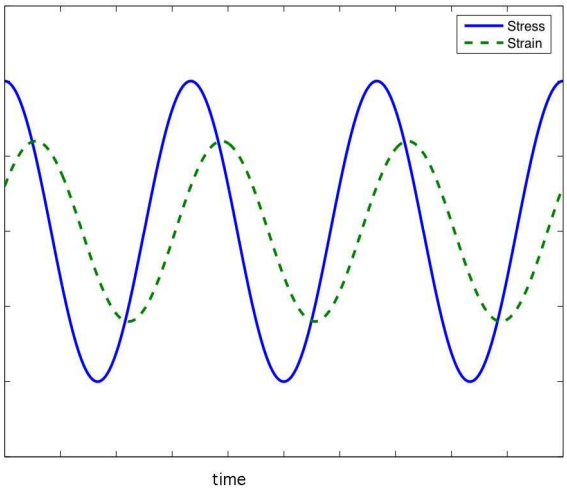

Figure 2.1: *Figure depicts the phase difference between stress and strain for sinusoidal deformation.*

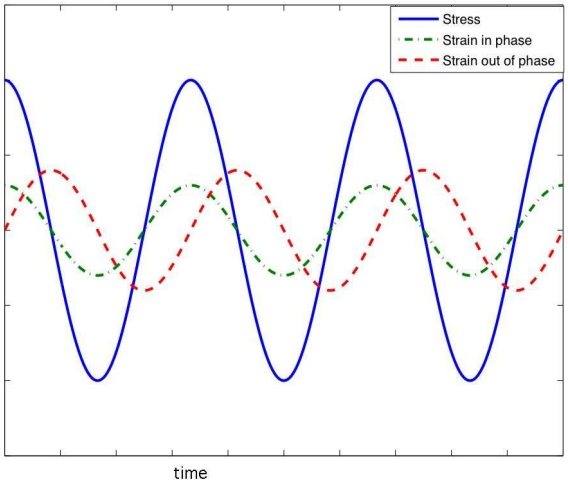

Figure 2.2: *Figure depicts the strain divided into 2 parts, one in phase and one $\frac{\pi}{2}$ radians out of phase with the stress.*

There are several ways of describing the stress-strain relationship, varying from very simple models as Maxwell and Voight models (see Figure 2.3) to more complex ones. Maxwell and Voight models both describes the material with two elements, one ideal spring and one dashpot (dissipative element). Maxwell's model puts them in series while Voigt's model puts them in parallel. More complicated methods are e.g. the fractional derivative model which states that the material damping is proportional to fractional derivatives of the displacement (Yuan and Agrawal 1998). All three models show different advantages in different situations, whereas Voight and Maxwell elements (or combinations of them) work for lesser degree of freedom systems (more degrees of freedom means large matrices to invert resulting in computational problems) in the frequency domain, the fractional derivative model is preferable in the time domain (where causality issues have to be considered) (Jones 2001).

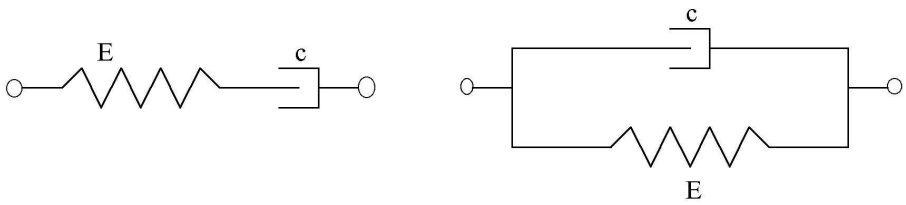

Figure 2.3: *(a) depicts Maxwell's viscoelastic model, E describes a springs and c a dashpot. (b) depicts Voight's viscoelastic model.*

2.2 Chemical composition of treads

Tread rubber can be a mixture of different types of rubber, e.g. ploybutadiene -, natural - and styrenebutadiene rubber (Andersson 2005). The rubber can be fused with vulcanizing chemicals, oils and filled with carbon black and silica. The purpose of the vulcanization is to impair the motion of the polymer chains at lower frequencies causing an increased stiffness. Fillers can be used in different proportions in order to change the ratio between the dissipative and the storing part of the modulus. The rubber samples used for testing in this thesis are polymer filled with black carbon. These composition is commonly used for road vehicle tires.

The material examined by the method is assumed to be homogenous and isotropic.

Even-though the processes in the making of the rubber compound can render slight anisotropy in the material. Traditional compression molding together with the proper blending of the ingredients is likely to produce non-homogeneity and anisotropy of negligible magnitude. The rubber is assumed to be nearly incompressible (i.e. ν=0.499), usually accepted when small hydrostatic stresses are considered. The strain dependence of the material parameters is neglected as only small strains are considered. Referring to Coja (2005), this is an adequate assumption to make for small dynamical strains in the audible frequency range.

2.3 Frequency-thermal zones of rubber

Frequency and temperature are tightly connected when it comes to their effect on the viscoelastic behavior of elastomers. It has been shown that a change in temperature can be described by a shift in frequency (Jones 2001). The complex modulus, of most polymer materials has got a significantly unlinear frequency response. To simplify the response the material is usually divided in to different frequency/temperature zones. These are referred to as the terminal-, the plateau-, the transition- and the glassy zone (see Figure 2.4). These names give a very good idea of the complex modulus behavior over frequency.

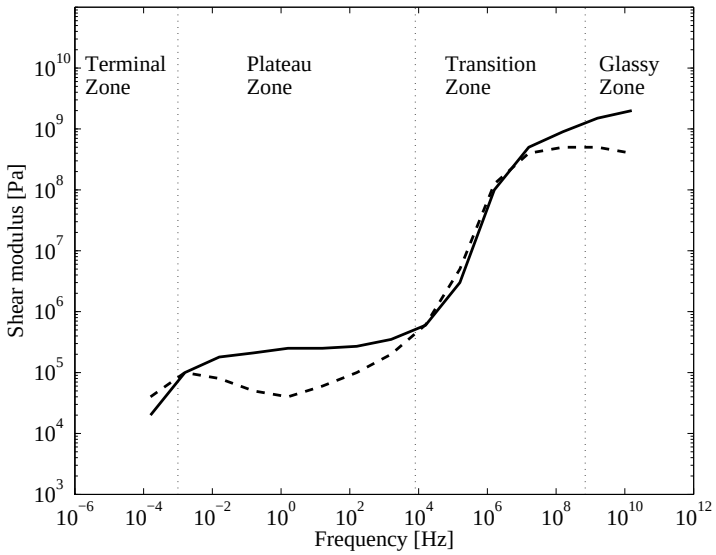

Figure 2.4: *Figure depicts the behavior of storage (solid line)- and loss modulus (dashed line) as functions of frequency. Figure taken from Andersson (2005).*

At the very low frequencies of the terminal zone the polymer chains can, because

of the long period time, move trough the entanglements completely rearranging their conformations. This causes high viscosity in the material thus a relatively high value of the loss modulus. This does not occur for strongly vulcanized, carbon filled elastomers (like tread materials) where the polymer chains are more fixed in their location.

When moving higher in frequency the terminal zone is replaced by the plateau zone. In the plateau zone, as the name indicates, the storage modulus stays comparably constant over frequency while the loss modulus suffers a minimum. This zone expands over the frequency range where most tread material property testing is conducted.

For the frequencies encompassed by the transition zone the time span is to short to allow sever configurational changes in the material. Thus the strain corresponding to a certain stress is less, compared to the plateau zone. The modulus increase with frequency. Most of the energy is dissipated as heat because of the increased friction between the polymer chains (Mark et al. 1994). The transition zone is characterized by the fact that the polymer is losing its elastomeric quality and is perceived, to become first leathery and then hard as frequency increases.

The extremely short period time at the high frequencies of the glassy zone prohibits all form of configurational changes, only local motions occur. The lag between stress and strain becomes shorter and the material acts less and less viscous. The material is perceived as "glassy".

Chapter 3

Traditional methods for determining material properties

Determining mechanical material properties of materials such as rubber treads has proven to be of a highly complicated nature. Especially dynamical properties when moving up in frequency. Testing methods can be separated into two subgroups, static and dynamic methods. Static methods, reveal a static stiffness commonly in the form of a modulus. Dynamic methods determine properties such as dynamic stiffness and dynamic losses (damping).

3.1 Static testing

Tensile stress-strain properties

Tensile stress-strain testing is probably the most common testing method of polymers mechanical properties (Brown 1999). The main reason for this ought to be the simplicity of the testing. The fundamental principle of the test is to stretch a sample until it breaks and measure the force and elongation, either continuosly or at various stages (see Figure 3.1). This test method provides you with information of the strength, elongation at break and modulus. The most common way is that the material samples are shaped in the form of dumbbells and placed in a machine that applies tension to the sample. One has to consider the change in cross section area of the specimen when conducting a test of this nature.

Compressional stress-strain properties

Compression measurements is obviously an appropriate method of evaluating material properties of rubber since there are many practical scenarios where rubber is used for its compressional characteristics. Like when it is being used as vibration isolation underneath heavy machinery. Despite this fact testing of this kind is far less common than tensile testing (Brown 1999). For a test like this it is of outmost importance that the test sample hight is very small in comparison with the compressed area, to avoid effects caused by buckling of the sample.

Shearing stress-strain properties

In opposite to tensile and compressional forces, which works perpendicular to the material surface, shear forces act parallel to the surface. Shear testing is not more difficult to perform than a tensile test and often the shear stress-strain relationship is linear for higher strains than the tensile strain-stress relation. Despite of this fact this test method is not often conducted (Brown 1999). This kind of test is conducted in order to get information about a materials shear modulus.

Flexural stress-strain properties

This type of testing is practiced almost as much as the tensile testing (Brown 1999). Its popularity is partly explained by the fact that the beam shaped geometry used is easier to produce than e.g. dumbbell. The test configuration is usually made up in one a the following ways; three- or four point loading or a simple clamped beam. The principal of the testing is to induce a flexural stress which gives rise to tensile stress on one side of the beam and compressive stress on the opposite side. The stress-strain relationship (most commonly the tensile) then leads to information about the modulus.

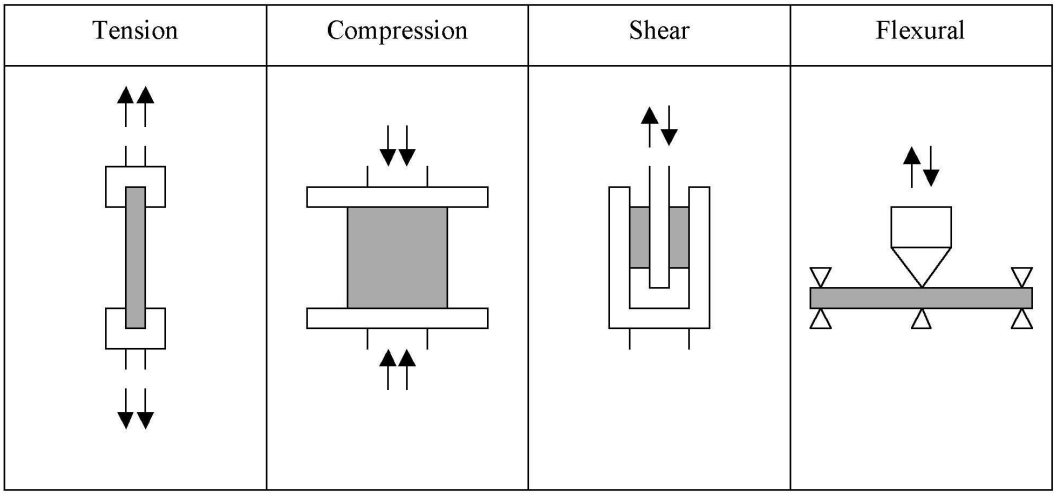

Figure 3.1: *Figure depicts schematically, how tensile, compression, shearing and flexural testing methods work.*

3.2 Dynamic testing

Vibrating beam configurations

The concept of vibrating beam configurations has been applied for several years. The principle of the technique is to vibrate a beam (consisting of material sample and some kind of boundary condition), collect and evaluate the data. There are different ways of evaluating the data depending, mostly, on the frequency range of interest. Some of the more common are "half power bandwidth" where the information at the resonance frequencies are considered or a one dimensional wave propagation. What they have in common though is there limitation at higher frequencies. The half power bandwidth method collapses when the resonances appear so close that the "half power range" include more than one resonance. A one dimensional wave propagation seize to work when, as the name implies, the propagation no longer can be considered as one dimensional.

Different beam configurations are frequently used. The most common ones are Oberst-, van Oort- or sandwich beam configuration (see Figure 3.2). The Oberst beam configuration is based on a multilayer cantilever beam consisting of the investigated material placed upon a rigid beam (steel,iron). Excitation and pickup are normally located at the free and of the beam. The cantilever configuration has been found to be the most effective way of avoiding several of the problems associated with other types of boundary conditions (Jones 2001). One possible problem with the Oberst beam is the asymmetry of the configuration. Thermal expansion happens at different rates in the investigated beam respectively the rigid beam which may cause bending problems at extreme temperatures. The van Oort beam reduces this problem by placing the investigated material on both sides a the rigid beam, thereby creating a symmetric configuration. When investigating softer materials or if a complex modulus is probed the sandwich beam configuration is common. The sandwich beam places the investigated material in between two rigid beams. Then the effect of bending of the inner layer can be neglected leading to simple equations for the evaluation (Jones 2001). All these configurations can be viewed in Figure 3.2.

3.3 ISO standards

In ISO 4664-1:2005 it is stated how testing of dynamical properties in rubber ought to be conducted. It states which types of apparatus should be utilized, how the laboratory conditions should be monitored. In the standard there are some assumptions, about the e.g. test equipment, that disables that the standard has followed during the development of the proposed method. There some paragraphs in the standard that can be followed within the framework of the proposed methods. This includes guidelines such as preconditioning of the test samples. The

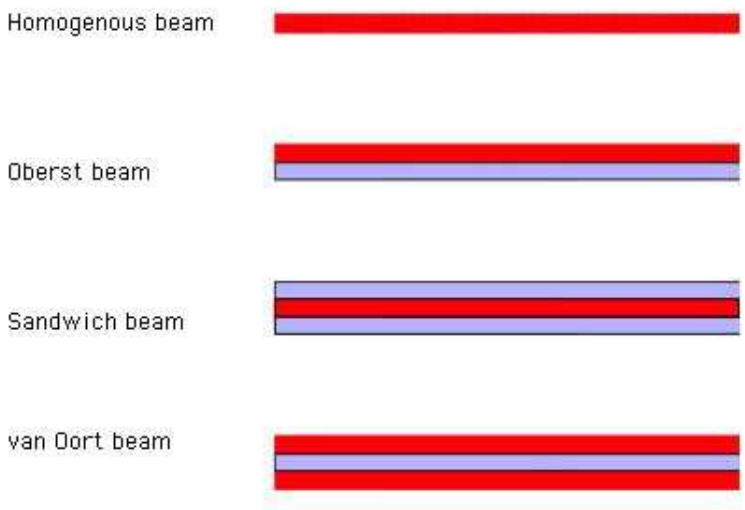

Figure 3.2: *Figure depicts a Homogenous beam (upper), an Oberst- (second upper), a sandwich beam (second lower) and a van Oort beam (lower).*

apparatus described in the standard is said to require the following elements:

a) Clamping or supporting arrangement that permits the test piece to be held so that it acts as the elastic and viscous element in a oscillating mechanical system.

b) Device for applying an oscillatory load (stress) to the test piece. The preferred for of impressed strain is sinusoidal, and the strain shall be impressed on the test piece with a harmonic distortion which is as low as possible, in no case greater than 10%

c) Detectors, for determining dependent and independent experimental parameters such as force, deformation, frequency and temperature.

d) Oven and controller, for maintaining the test piece at the required temperature.

e) Instrumnets for measuring test piece dimensions, in accordance with ISO 23529.

Item a) an b) are basic conditions for all types of dynamic property testing of rubber. Naturally these conditions are met by the proposed method. A temperature controlled laboratory has not been used during the test presented in this thesis but

the method itself does not prohibit it. Test pieces can be prepared and conditioned in accordance with ISO 23529:2004, although that is not necessarily the case for the test procedure within the limits of this thesis.

3.4 Limitations of traditional methods

The presented methods are not sufficient especially at high frequencies, consequently new methods are frequently being developed and evaluated. Most methods normally show a severe limitation in their valid frequency ranges due to that they evaluate the material response at resonance frequencies, i.e. at high frequencies resonances appear in all dimensions making it difficult to distinguish the resonances. Highly damped materials is also problematic to evaluate at resonances since the resonance peaks become broader and it can be hard to distinguish them from each other. Another problem commonly associated with traditional testing methods is to avoid loading the material (with e.g. an accelerometer) when measuring the response of them. Figure 3.3 show a typical mobility as function of frequency. It is clear that the resonances are hard to distinguish when frequency increases.

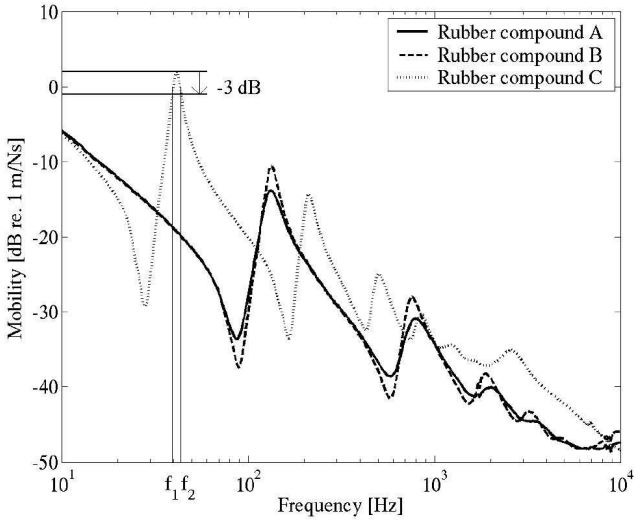

Figure 3.3: *Figure depicts a typical mobility plot. The half power bandwidth is indicated. At higher frequencies the resonance frequencies become harder to clearly define. Figure taken from Andersson (unpublished)*

Chapter 4
Velocity profile matching method

The velocity profile matching method (VPMM), first mentioned in Andersson (2005), is the purpose of this thesis and it proposes a way of acquiring stiffness and damping out of rubber compounds. The method is based on a velocity profile match between measured- and numerically modeled data. A rubber sample is excited with a sinusoidal signal fed mechanical shaker and the response is measured along the centerline with a laser Doppler vibrometer (LDV). The calculated velocity profile is the results of a finite-element model of the rubber sample used for the measurements. The material parameters, stiffness and damping, are updated until a least squared error between measured- and calculated results is achieved. The updating process is governed by either a descent algorithm or a grid search.

4.1 Physical principles of the method

The fundamental principle of this method is that a finite-element model gives the vibration pattern of a rubber sample with such high precision so that, when compared with measured results, the dynamic properties of the material can be extracted from the models. The intention is to excite a rubber sample with a sinusoidal mechanical excitation and measure the velocity along the center line of the top surface of the sample (see Figure 4.1). The measurements should be done without interfering with the vibrational pattern of the sample. A finite-element model is then created in a computer software. Boundary information from the measurements are used in order to get a correctly modeled boundary condition. The finite-element model ought to be solved for the same frequency that is used for the sinusoidal excitation in the measurement setup. A top surface, center line velocity profile is interpolated from the nodal point values of the finite-element solution. This velocity profile is then compared with the measured equivalence, yielding an error. The error is the sum of all the discrete point deviations squared, along the velocity profile. The material parameters in the finite-element model are adjusted and a new error is computed. This process continues until the error converges to a minimum value. The material parameters used to create the solution yielding the least error is the method's estimation of the material parameters in the rubber sample (see Figure 4.2).

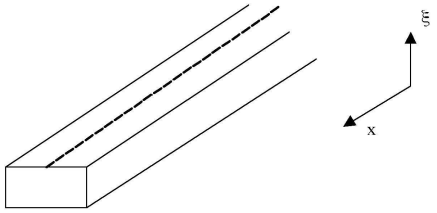

Figure 4.1: *Figure depicts top surface, centerline.*

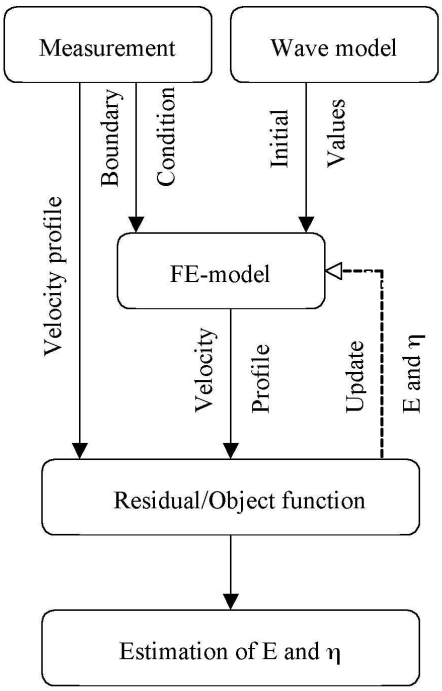

Figure 4.2: *Flow chart describing the process of estimating the material parameters based on gradient search method.*

4.2 Modeling

4.2.1 Finite Element Method

Theory

The finite element method (FEM) is, as the name implies, a way of breaking down problems into finite sized "elements". There is a physical phenomenon which is described by a set of differential equations, that might not have or where it is hard

to obtain an analytical solution. This set (could extend from one to several) of differential equations is broken down into finite element equations. If these are chosen well, they ought to provide a good approximation to the original set of equations (see Figure 4.3). Even though the differential equation might vary in a highly non-linear way over a certain domain it might be reasonable to assume that over a sufficiently small region it behaves linearly (or quadratic etc.). The elements

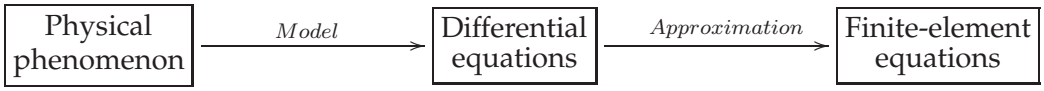

Figure 4.3: *Schematic figure showing the steps from reality to numerical approximation.*

are characterized by so called shape functions. Those functions describe how the investigated quantity behaves over the element. Shape functions are polynomials of chosen order (see Figure 4.4). The elements are assigned discrete values only at its nodes. How many nodes an element has got depends on the element shape function and the geometry of the element. Elements that are described by a first order polynomial has only got nodes (numerical values) at its corners (ends if it is 1-D), and between them the investigated quantity varies linearly. Thus, the higher order polynomial describing the shape function of an element the closer the finite element solution is to the analytical solution of the modeled problem. Although with higher order polynomials the computational cost also increases. The elements are only linked to each other trough their boundaries, i.e. nodes at the vertices of an element is shared by the neighboring elements. This is an important feature of the method, each element is only connected to its neighbor elements. The system of elements is collected in large matrices describing the relevant properties of the elements. For example a solid mechanics problem could utilize matrices describing properties such as, mass, stiffness and damping. Because each element is only connected to its neighboring elements the system matrices are sparse and banded (only a band around the matrix diagonal are populated by values that differs from zero) which is a significant advantage in terms of computational cost. The solution of the finite-element model, is only given at the nodes. A solution at any other point (which is not a node) must be interpolated between nodal point values.

A structural mechanical problem can provide three types of relations which information can be benefited from. They are constitutive properties, kinematic relations and equilibrium conditions. They are connected as shown in Figure 4.5. Since there is no structural information the solution process has to go from external load through the stress and the strain to the displacement which is the desired information. The equilibrium condition, together with kinematic- and constitutive relations yields the differential equation which can be modeled with finite-element technique (see *Appendix A*).

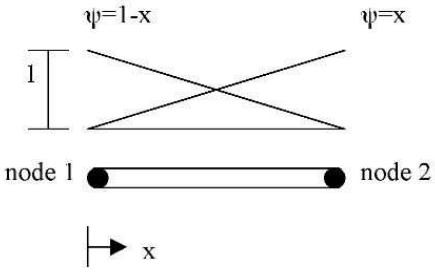

Figure 4.4: *Figure depicts a one dimensional, first order element. The shape functions vary linear over the element.*

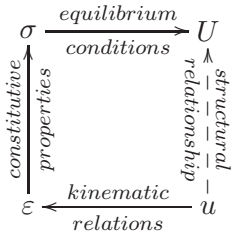

Figure 4.5: *Figure depicts how displacement (u), strain (ε), stress (σ) and external load (U) are connected.*

Implementation

The finite-element model was constructed in MULTIPHYSICS. A commercially available software from Comsol. The rubber beam was modeled with solid elements in a block with the dimensions of the rubber sample. Quadratic Lagrange elements, with linear viscoelastic properties were selected. Quadratic means that the element shape functions are represented by a second order polynomial. This implies that nodes exist within the element as opposed to just on the element boundaries as for a linear element. The term "Lagrange" indicates that the polynomials describing the shape functions are found trough the Lagrange interpolation formula (Ottosen and Petersson 1992). Sufficient discretisation in the finite-element mesh was chosen as to be greater than ten nodes per wavelength. This gives the maximum element size for the model. The mesh is then constructed by an algorithm in MULTIPHYSICS (see Figure 4.6).

The control mass was modeled as ablock with high stiffness and little damping in order to get approximately a rigid rotation. The dimensions of the control mass was set as; 10 mm x sample width x sample thickness. This saves a computational cost compared to modeled the mass with its real dimensions, and the effect on the

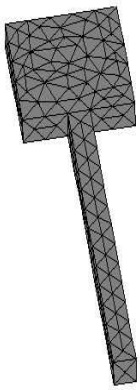

Figure 4.6: *Figure depicts the meshed finite element model. This model includes the full dimensions of the control mass, not used in the calculation process but included here for easy separation between control mass and sample.*

velocity profile is considered as negliable. The boundary conditions were given as displacements on each edge of the control mass. These displacement were taken directly from the measurement data. From the solved finite element model the center line velocity profile was interpolated using MatLab function postinterp.m.

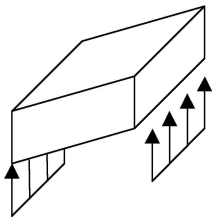

Figure 4.7: *Figure depicts how the measured displacements were given as boundary conditions on the edges of the control mass.*

The damping in the finite-element model is implemented as Rayleigh damping (standard in the software). Rayleigh damping means that the damping is considered to be proportional to the stiffness- and mass matrix of the solution. It is defined as two proportionally constants, one for stiffness respectively mass. If in the model the mass proportionally constant (c_M) is set to zero, the damping can be stated as a loss factor (η) divided by the investigated angular frequency instead

of a stiffness proportionally constant (c_K) [1]. Considering the equilibrium equation (see *Appendix A*),

$$(-\omega^2\mathbf{M} + j\omega\mathbf{C} + \mathbf{K})\mathbf{u} = \mathbf{R}, \tag{4.1}$$

and replacing the damping term $\mathbf{C}$ with the Rayleigh damping model according to,

$$(-\omega^2\mathbf{M} + j\omega(c_M\mathbf{M} + c_K\mathbf{K}) + \mathbf{K})\mathbf{u} = \mathbf{R}. \tag{4.2}$$

Following the reasoning above (c_M =0 and $c_K = \frac{\eta}{\omega}$) equation 4.2 yields,

$$(-\omega^2\mathbf{M} + \mathbf{K}(1 + \eta j))\mathbf{u} = \mathbf{R}. \tag{4.3}$$

Thereby the stiffness matrix ($\mathbf{K}(1+\eta j)$) has complex notation which includes both stiffness and damping according to viscoelastic theory.

4.2.2 Wave model

The normal surface displacement can be described as the sum of four components when considering a one dimensional wave propagation, i.e. if only bending waves are considered. That is normally acceptable because they are the main contributors of normal displacement. This approach also assumes that the beam can be considered as infinite, i.e. reflections from boundaries are not included. These four components are, a wave traveling in positive direction, a wave traveling in negative direction and respective near fields. Near fields are exponentially decaying local deformations that do not transport energy. They occur at excitation points and boundaries. Hence, the normal displacement (ξ) can be expressed as a function of time and x-coordinate,

$$\xi(x,t) = [\xi_+ e^{-jkx} + \xi_- e^{-jkx} + \xi_{+j} e^{kx} + \xi_{-j} e^{kx}]e^{j\omega t} \tag{4.4}$$

Considering time invariant conditions it is possible to neglect the time function and the normal displacement reduces to a function depending only on the length direction of the beam (x). In order to get the unknown amplitudes ([ξ_+ ξ_- ξ_{j+} ξ_{j-}]^T) it is necessary to formulate four equations (as many as there are unknowns). The information benefited from the boundary conditions can be used. The displacement and the rotation at one end of the beam are known from measurements and at the free end of the beam the force and the moment is zero. Considering small rotation angles, displacement and rotation are connected as,

$$\beta(x) = \frac{\partial\xi(x)}{\partial x} \tag{4.5}$$

[1] In the FemLab software these proportionality constants are called α and β, but that notation are used for other purposes in thesis thesis.

Similarly there also are relations, trough constitutive relations, between rotation and moment (equation (4.6)) and moment and force (equation (4.7))

$$M(x) = -B\frac{\partial\beta(x)}{\partial x} \tag{4.6}$$

$$F(x) = B\frac{\partial M(x)}{\partial x} \tag{4.7}$$

where B denotes bending stiffness. Applying equation 4.4 to our rubber sample using the relations above yields the equation system below,

$$\begin{pmatrix} 1 & 1 & 1 & 1 \\ -j & j & -1 & 1 \\ je^{-jkL} & -je^{jkL} & -e^{-kx} & e^{kx} \\ -e^{-jkL} & -e^{jkL} & e^{-kx} & e^{kx} \end{pmatrix} \begin{pmatrix} \xi_+ \\ \xi_- \\ \xi_{j+} \\ \xi_{j-} \end{pmatrix} = \begin{pmatrix} \xi = \xi_0 \\ \xi = \beta_0/k \\ \xi = F/k^3 = 0 \\ \xi = M/k^2 = 0 \end{pmatrix}$$

where ξ_0 is the measured displacement and β_0 the measured rotation.
This model is usually based on so called Euler-Bernoulli beam theory. This framework assumes that the cross section rotates stiffly, perpendicular to the natural axis of the beam and that the rotational angles are small. This theory normally works fine (the error does not exceed 10 %) when the wave propagation in the beam mainly occurs in its length direction. Although when the wavelengths become approximately in the order of six times the cross sectional dimensions (which ever of the dimensions is smallest) it is normally no longer sufficient (Cremer and Heckl 1987). There are other frameworks that incorporate certain consideration of the cross section thereby allowing smaller wavelengths (higher frequencies). One of them is Timoshenko beam theory which still assumes a stiff cross section but does no longer require it to be perpendicular to the neutral line, as assumed by the Euler-Bernoulli theory.

4.3 Measurements

4.3.1 Sample preparation

The sample pieces were cut with a water-jet cutter. An extremely high pressured stream of water that, together with abrasive, cuts through the raw rubber tread pieces. The samples were cut into three different sizes (see Figure 4.9) referred to as A, B and C. Five specimens of each sample size were cut. The sample cutting took place at Chalmers Waterjet Lab at Chalmers Lindholmen. Figure 4.8 (a) shows the process of the high pressure water-jet cutting trough one of the rubber "plates" into the desired dimensions. In Figure 4.8 (b) the cage in which the process took place can be viewed.

(a) (b)

Figure 4.8: *(a) shows the water jet cutter in the progress of cutting a sample. (b) shows the encapsulation from the outside.*

Figure 4.9: *The different sample sizes, from the left A, B and C*

Sample	length	width	thickness
A	130	9.60	6.50
B	84.0	145	10.0
C	130	3.60	2.20

Table 4.1: *The table shows the dimensions, in mm, of the different sample sizes.*

The samples were cut into the dimensions presented in Table 4.1. Two samples of each size were selected and dived into two groups. These groups will be referred to as measurement set one and measurement set two. The same measurements were performed for booth sets (see Table 4.2)

Freq [hz]	500	750	1000	1500	2000	2500	3000	3500	4000	4500	5000
A	√	√	√	√							
B			√	√	√	√	√	√	√		
C								√	√	√	√

Table 4.2: *The table shows which samples were intended to be measured and at what frequencies.*

4.3.2 Setup

The aim of the measurements were to acquire velocities as function of the beams length direction, for single frequencies. A mechanical shaker was attached with its backside on a rigid object. The mechanical shaker was fed with sinusoidal signals at different frequencies. A force transducer was placed between the control mass and the mechanical shaker. The stinger connecting the shaker and the force transducer were made short enough to disable stinger resonances in the considered frequency range. The force transducer provided information of the magnitude of the applied force and works as a reference for the phase, although only amplitudes are considered in the velocity profile comparison. At the lower end of the control mass the rubber tread sample was attached (See Figure 4.10 and Figure 4.11). The control mass was suspended by springs to decouple it from the rest of the set up, in terms of vibrations. The velocities along the center line on the top surface of the sample was measured with a laser Doppler vibrometer. The measurements were conducted in a laboratory assuring a temperature of 22 ± 0.5 ° C. Due to relatively short testing periods and small strain amplitudes the vibration induced heat increase in the sample was assumed to have an insignificant effect on the materials viscoelastic properties. Measurements were conducted in order to investigate the temperature rise in the sample during excitation. A temperature probe was inserted in a sample piece and the heat increase over time was recorded for a sample excited with a large amplitude at 1000 Hz. The temperature increase proved to flatten out after approximately an hour and the rise was so small that its effect was considered negligible. Although exciting the sample with higher frequencies would most certainly effect the temperature rise greater, the effect was considered to still be negligible.

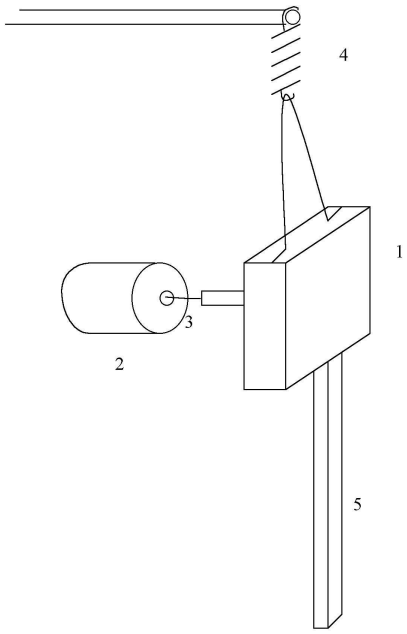

Figure 4.10: *Scematic drawing showing the measurements setup. 1. Control mass. 2. Meachanical shaker. 3. Stinger and force transducer. 4. Spring. 5. Sample.*

Figure 4.11: *Figure shows a picture of the measurements setup*

4.3.3 Measuring boundary conditions

To in a controlled matter be able to define the boundary in which the sample is attached in the excitation point, a control mass is introduced. The excitation of the beam cause certain rotational motion of the sample as oppose to only translatory motion (see *Section 4.5*). Thus, this rotation also has to be modeled as a boundary conditions in the finite element model. The control mass has and approximately rigid rotation in the considered frequency range (see Figure 4.12). Thus, if it is possible to measure the displacement of the mass over a certain distance it is possible to obtain the rotational angle. The displacement (ξ) at a certain point subtracted with the displacement at another point yields, through a trigonometrical relation, the bending angle according to,

$$\beta = \arctan\left(\frac{\xi(x_2) - \xi(x_1)}{x_2 - x_1}\right) \tag{4.8}$$

where x_1 and x_2 are two measurement points.

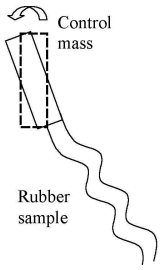

Figure 4.12: *The control mass rotates stiffly while the rubber sample deforms according to a vibrational pattern.*

4.3.4 Limitations

Due to noise

Nodes are the points on a vibration pattern that during vibration remain still. Thus the regions around the nodes have low vibration amplitude. In these regions the signal to noise ratio is poor. At a certain level the signal is as low as the noise, hence vibration amplitudes of this order cannot be registered.(Figure 4.13) This limitation due to noise level is considered when defining the error between calculation and measurement, see *Section 4.4*.

Due to discretization

The measurement points along the rubber sample were chosen with approximately one millimeter between them. Due to the distance between the discrete measure-

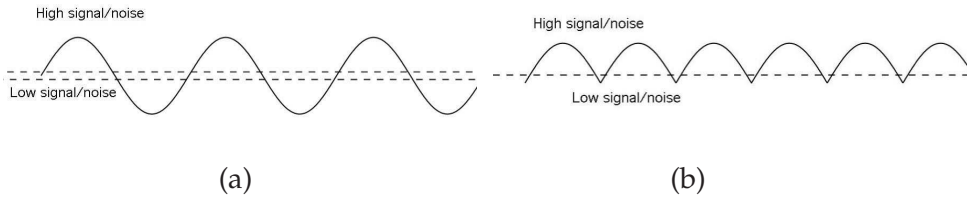

Figure 4.13: *(a) depicts the wave pattern on the beam, the dashed lines indicates the noise level. (b) depicts the vibration amplitudes, the dashed line indicates the noise level.*

ment point errors can occur in the mismatch between measurement and calculation in agreeing were the control mass ends and where the rubber sample begins. The first measurement point on the rubber sample can be determined within a precision of plus/minus half the distance between two measurement points. This differentiation is done by ocular inspection by examining the measurement data. This effect ought to mainly effect the estimation of the Young's modulus due to the fact that it is mainly the stiffness that controls the spatial aspect of the velocity profile. This means that the measured and calculated velocity profiles may be, at the maximum, shifted $\pm.5$ mm along the x-axis. Making the material appearing less or more stiff than what it actually is. This effect ought to be minimized though by repeating the measurements a sufficient number of times. Calculations reveal this mismatch problem to yield a Young's modulus error of less than the 10% confidence interval that was aimed at. The error in the loss factor is insignificantly small.

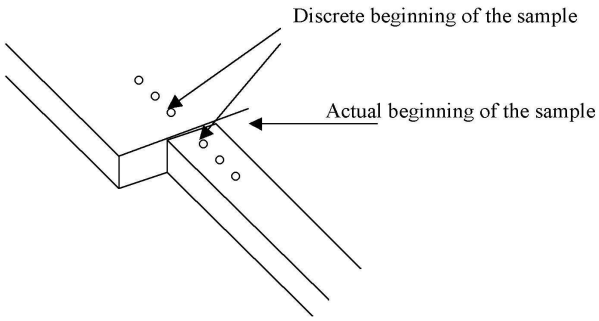

Figure 4.14: *Figure depicts the possible mismatch measurement points and actual beginning of the beam.*

4.3.5 Primary evaluation of measurement results

Before analysing the measurement results and comparing them to modeled results a primary review of the measurements were made. It clearly showed that the results for sample C turned out to be severely influenced by noise (see Figure 4.15). It is difficult to see a clear vibration pattern on the sample. This ought to be because at this frequency the vibration is greatly damped close to the free end of the sample. Therefore, the sample C was cut into a new sample size. Keeping its cross sectional dimension the length was reduced to 600 mm. The measurements where repeated for the frequencies originally intended for sample C (i.e. 3500-5000hz). Only one measurement set was conducted for this reduced sample C. Thus, results for sample C are not included in measurement set one and measurement set two in *Chapter 5* but instead as a third measurement set; Measurement set reduced sample C.

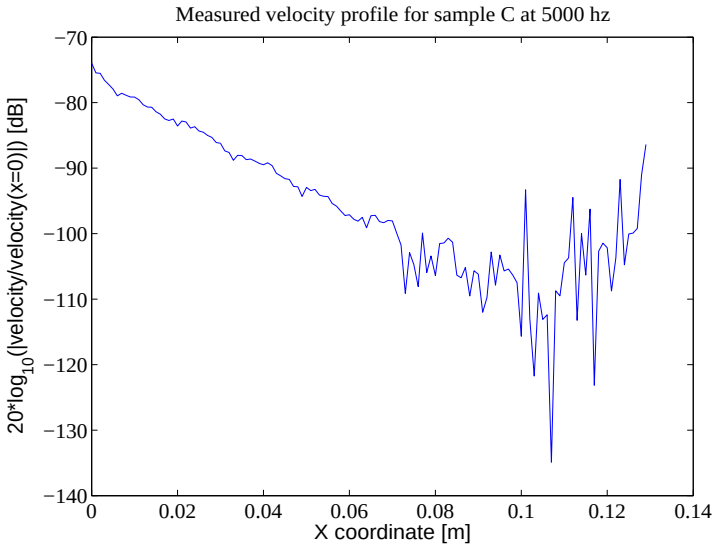

Figure 4.15: *Figure depicts the measured velocity profile for sample C at 5000hz.*

Freq [hz]	3500	4000	4500	5000
Reduced C	√	√	√	√

Table 4.3: *The table shows at which frequencies reduced sample C was measured.*

4.4 Algorithms for updating material parameters

4.4.1 Object function

To obtain the best possible fit between the velocity profiles, the measured ($\mathbf{v}^{\text{meas}}$) and the numerically modeled ($\mathbf{v}^{\text{calc}}$), the error between them ought to be minimised. The error between them (z) is defined as the sum of all velocity discrepancies squared and weighted according to,

$$z = \sum_{i}^{I} |v_i^{\text{meas}} - v_i^{\text{calc}}(E, \eta)|^2 W_i, \tag{4.9}$$

where i denotes the discrete points in the length dimension of the beam. The weight function ($\mathbf{W} = [W_1, W_2, \dots W_I]^T$) is supposed to compensate for the problems with low signal to noise ration close to bending nodes. That means errors in points with high signal to noise ration is more significant to the total error than error in points with low signal to noise ratio. The weight function was chosen as,

$$\mathbf{W} = \frac{|\mathbf{v}^{\text{meas}}|}{\max(|\mathbf{v}^{\text{meas}}|)}. \tag{4.10}$$

Where $\mathbf{v} = [v_1, v_2, \dots, v_I]^T$. The weight was changed to a unit vector ($\mathbf{W} = [1, 1 \dots, 1]$), of size I, at higher frequencies due to that vital information about wave pattern that occurs close to the free end is otherwise disregarded by the descent algorithm.

4.4.2 Descent algorithms

The function described in equation (4.9) is the object (natural merit) function which is to be minimized. Since $\mathbf{v}^{\text{calc}}$ is a function of the material parameters E and η, if everything else is kept constant in the finite-element model and ($\mathbf{v}^{\text{meas}}$) is a constant, z is also a function of E and η; z=f(E,η) $\Re^2 \rightarrow \Re$. Thus the goal is to to minimize a two dimensional real valued function. To, in an intelligent manor, update E and η and thereby finding the global minimum of the object function, a gradient algorithm is implemented. The most known gradient algorithm is the steepest descent algorithm invented by Cauchy more than 100 years ago. The main concept of the algorithm is to find the gradient of a function and from there, seek a smaller (larger) function value in the direction of the gradient. This process is continued until a minimum (maximum) is found. First the search direction is chosen according to,

$$\mathbf{h}_i = -\nabla \mathbf{z}(\mathbf{p}_i). \tag{4.11}$$

Then the parameters are updated as,

$$\mathbf{p}_{i+1} = \mathbf{p}_i + \alpha_i \mathbf{h}_i. \tag{4.12}$$

Where the step size (α) is computed, satisfying the following criteria;

$$\alpha_i \in \alpha(\mathbf{p}_i) \triangleq \arg(\ \min(z(\mathbf{p}_i + \alpha \mathbf{h}_i))), \alpha \geq 0 \tag{4.13}$$

A problem with this kind of algorithm is that its step size criteria (equation (4.13)) is difficult to implement (Polak 1917). When this algorithm was implemented a constant step-size (α) was used. Another problem with the steepest descent algorithm is the fact that each new search direction is orthogonal to the previous one, causing the algorithm to oscillate heavily (see Figure 4.16). As a result, the algorithm can leap back and forth and thereby leading to slow convergence or stepping over the minimum. A simple way to avoid the oscillations commonly as-

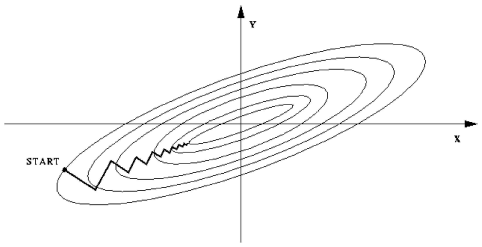

Figure 4.16: *Figure depicts the oscillating motion of the steepest descent algorithm.*

sociated with the steepest descent algorithm is to add a momentum term, resulting in something called gradient descent algorithm. This means that instead of each new search direction being orthogonal to the previous one it is a compromise of the two. The search direction results in,

$$\Delta \mathbf{p}_i = \mathbf{h}_i + \Delta \mathbf{p}_{i-1}. \tag{4.14}$$

A desired part (γ) of the momentum is added to the search direction of steepest descent resulting in,

$$\mathbf{p}_{i+1} = \mathbf{p}_i + \gamma \alpha \mathbf{\Delta} \mathbf{p}_i \tag{4.15}$$

The momentum term can be arbitrarily chosen between zero and one. Using a slightly more sophisticated method of choosing the search direction can be done by choosing the term γ according to Fletcher and Reeves,

$$\gamma_{i+1} = \frac{\mathbf{h}_{i+1}^t \mathbf{h}_{i+1}}{\mathbf{h}_i^t \mathbf{h}_i} \tag{4.16}$$

or to Polak and Ribiere (Heath 2002).

$$\gamma_{i+1} = \frac{(\mathbf{h}_{i+1} - \mathbf{h}_i)^t \mathbf{h}_{i+1}}{\mathbf{h}_i^t \mathbf{h}_i} \tag{4.17}$$

More detailed information about the descent algorithms can be found in Polak (1917) or Heath (2002).

The parameters of the optimization models were tuned to values appropriate for the intended calculation process. The descent algorithms (both steepest descent and gradient descent) was implemented in Matlab. The finite-element model was made as a function that was called from a m-file containing the descent algorithms see Figure 4.17.

READ input and measurement data

Initial guess: *Call Wave Model* $\mathbf{p}_{i-1}$
Compute objective function: *Call MULTIPHYSICS* $\mathbf{z}_{i-1}$=$|\mathbf{v}^{\mathrm{meas}}$-$\mathbf{v}^{\mathrm{calc}}(\mathbf{p}_{i-1})|^2$

LOOP i=1,2,. . . ,n
Calculate gradient: $\nabla\ \mathbf{z}_{i-1}$
Update coefficients: $\mathbf{p}_i \leftarrow \mathbf{p}_{i-1}$
Solve FE-model: *Call MULTIPHYSICS* $\mathbf{v}^{\mathrm{calc}}(\mathbf{p}_i)$
Compute objective function: $\mathbf{z}_i$=$|\mathbf{v}^{\mathrm{meas}}$-$\mathbf{v}^{\mathrm{calc}}(\mathbf{p}_i)|^2\ \mathbf{w}$
END

Figure 4.17: *Figure depicts the implementation of the steepest descent algorithm.*

4.4.3 Grid searches

A grid search is a fairly simple minimisation technique. The principle is to give a highest and a lowest value of the function variables, ($\mathbf{p}_{\min}$ $\mathbf{p}_{\max}$) build a large matrix and locate the combination which yields the least error (in some meaning). This search can continue by making a new matrix around that minimum value in order to seek a global minimum. Mathematically this is described, for the case of $\mathbf{p} \in \Re^2$, according to

$$\min(\mathbf{z}) = \min \begin{pmatrix} z(p_{1,1}) & z(p_{1,2}) & \dots & z(p_{1,n}) \\ z(p_{2,1}) & z(p_{2,2}) & \dots & z(p_{2,n}) \\ \vdots & \vdots & \ddots & \vdots \\ z(p_{n,1}) & z(p_{n,2}) & \dots & z(p_{n,n}) \end{pmatrix}. \tag{4.18}$$

Where $\mathbf{z}$ is quadratic matrix containing the errors that arise when using the variables in $\mathbf{p}$. The routine that performed these mathematical operations were programmed in Matlab.

4.5 Primary work

Some work was performed in order to finalize the method to the manner in which it is presented in this chapter. This section provides a short summary of the work and discarded ideas leading to the final method.

In the first measurement setup there was no control mass, instead the rubber sample was mounted directly on an impedance head [2] (see Figure 4.18). This proved to cause difficulties in the comparison process that matches the measured- with the numerically modeled velocity profile. It turned out that the velocity profiles never matched close to the excitation point, making it impossible to fit them without excluding this part. When excluding the points close to the excitation, vital information is neglected and results are no longer dependable. The impedance head does not just transfer the translatory translative force from the shaker. There is also a bending stiffness of unknown magnitude created in the excitation point. In the finite-element model the rotation, caused by the bending stiffness was not included which gave rise to this mismatch problem close to the excitation point. Hence the control mass was included in the measurement setup. Figure 4.19 shows the problem close to the excitation point due to the rotation. It also shows that in the early stages of the development, the method was dealing with mobility profiles due to that force, in stead of displacement, were given as boundary condition in finite element model.

Attempts were made in order to implement more sophisticated methods in choosing proper step sizes for the descent algorithm. The step size were to be chosen as the first number in an series of $(\frac{1}{2})^n, n = 0, 1, 2, \ldots, m$ to satisfy the Armijo criterion as done in Dussault (2000). This idea had to be discarded though due to the large computational cost when the finite-element model had to be solved several additional times in each iteration just to "optimize" the step size. Instead in the final Matlab-script where the algorithm was implemented a constant predefined step size is used. This is not believed to compromise the results of the minimisation, only the computation time of process.

[2] Measurement device that measures both velocity and applied force in the mounting point. Force divided by velocity equals mechanical impedance.

Figure 4.18: *Figure depicts the measurement setup which had the rubber sample placed directly on an impedance head.*

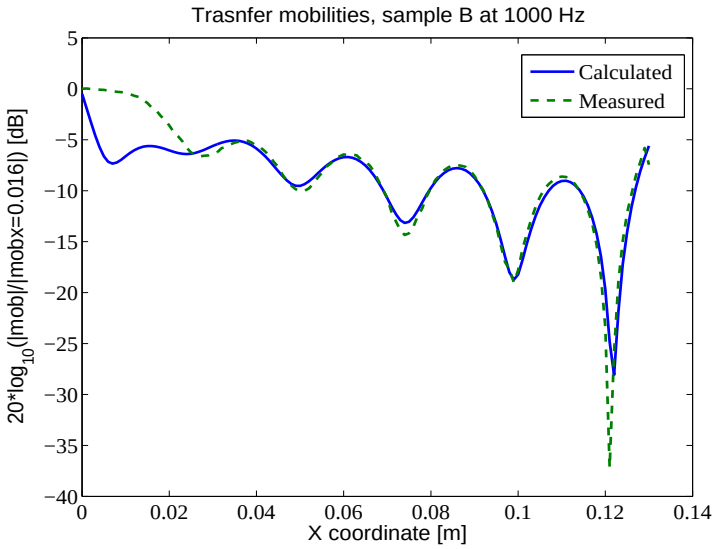

Figure 4.19: *Figure depicts the obvious mismatch of transfer moblilities close to the excitation point, located where x is zero.*

Chapter 5
Results

5.1 Dynamic modulus and loss factor

All calculated material parameters for measurement set one, measurement set two and measurement set reduced sample C are presented both in a plot and a table. Due to unknown reasons the measurement at 2000 Hz, for measurement set one, turned out to show only noise. Due to noise for sample C in measurement set one and measurement set two no results are produced for them.

Measurement set: 1

Sample size	**A**		**B**		**C**	
Freq [hz]	E [MPa]	η [-]	E [MPa]	η [-]	E [MPa]	η [-]
500	44.8	0.162				
750	45.6	0.245				
1000	49.8	0.257	55.0	0.257		
1500	51.0	0.301	57.0	0.315		
2000						
2500			51.3	0.322		
3000			53.8	0.351		
3500			54.2	0.368		
4000			58.8	0.393		
4500						
5000						

Table 5.1: *Table show the material parameters for the frequencies and samples for which it was possible to produce results. For measurement set 1.*

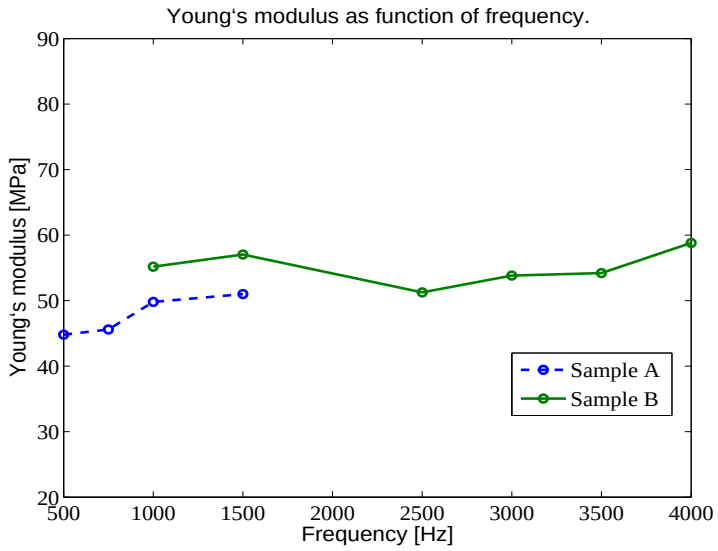

Figure 5.1: *Figure depicts Young's modulus as a function of frequency.*

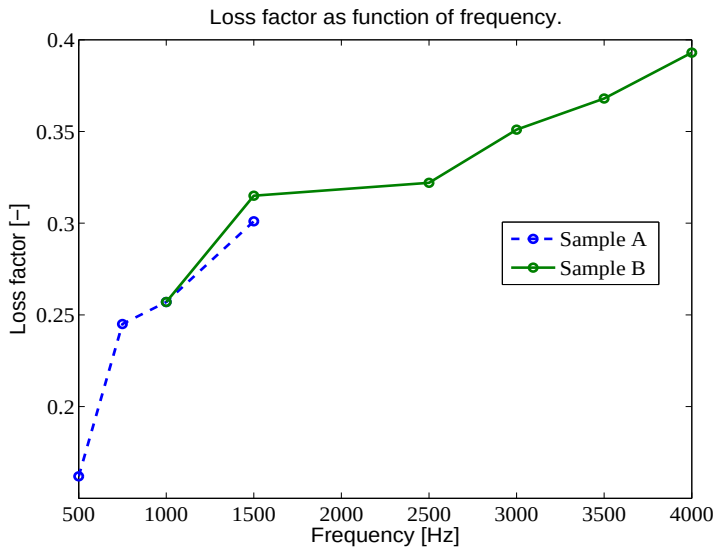

Figure 5.2: *Figure depicts loss factor as a function of frequency.*

Measurement set: 2

Sample size	**A**		**B**		**C**	
Freq [hz]	E [MPa]	η [-]	E [MPa]	η [-]	E [MPa]	η [-]
500	41.5	0.164				
750	45.7	0.232				
1000	46.0	0.233	65.0	0.241		
1500	52.5	0.286	68.2	0.270		
2000			71.5	0.294		
2500			77.9	0.309		
3000			78.3	0.346		
3500			71.0	0.360		
4000			74.0	0.384		
4500						
5000						

Table 5.2: *Table show the material parameters for the frequencies and samples for which it was possible to produce results. For measurement set 2.*

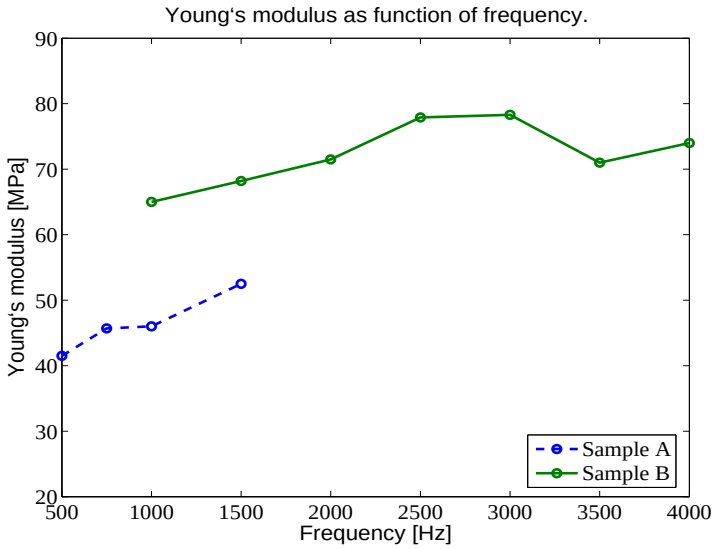

Figure 5.3: *Figure depicts Young's modulus as a function of frequency.*

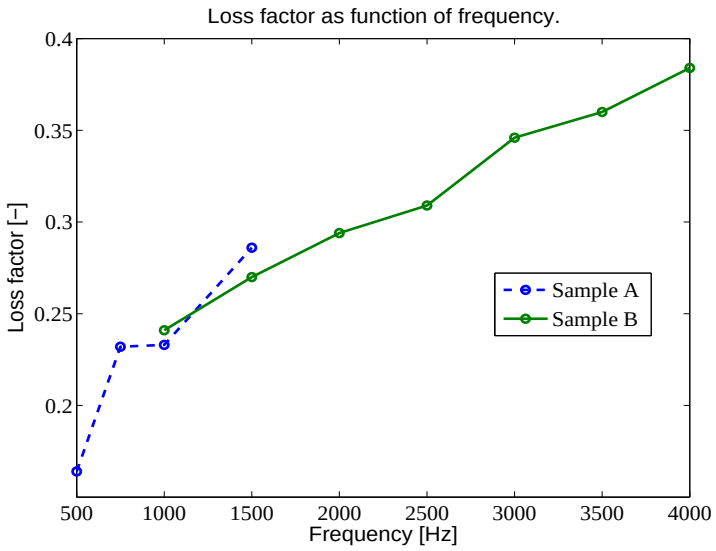

Figure 5.4: *Figure depicts loss factor as a function of frequency.*

Measurement set: reduced C

Sample size	**Reduced C**	
Freq [hz]	E [MPa]	η [-]
3500	69.0	0.337
4000	72.8	0.345
4500	70.7	0.360
5000	73.0	0.376

Table 5.3: *Table show the material parameters for the reduced sample C.*

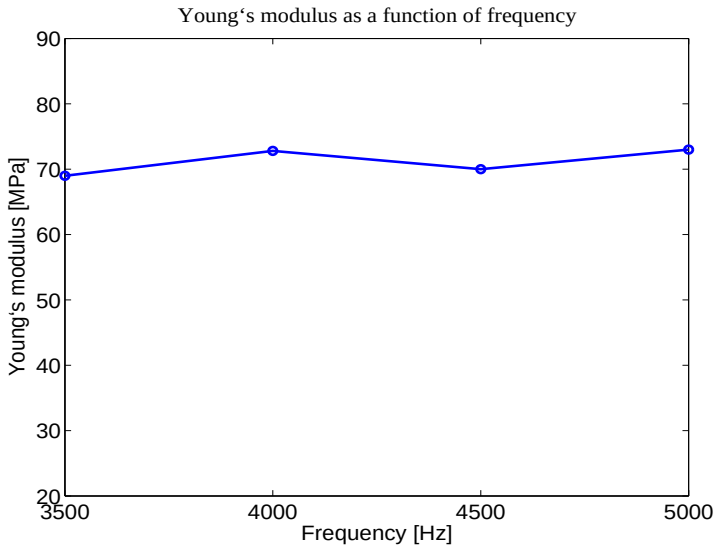

Figure 5.5: *Figure depicts Young's modulus as a function of frequency.*

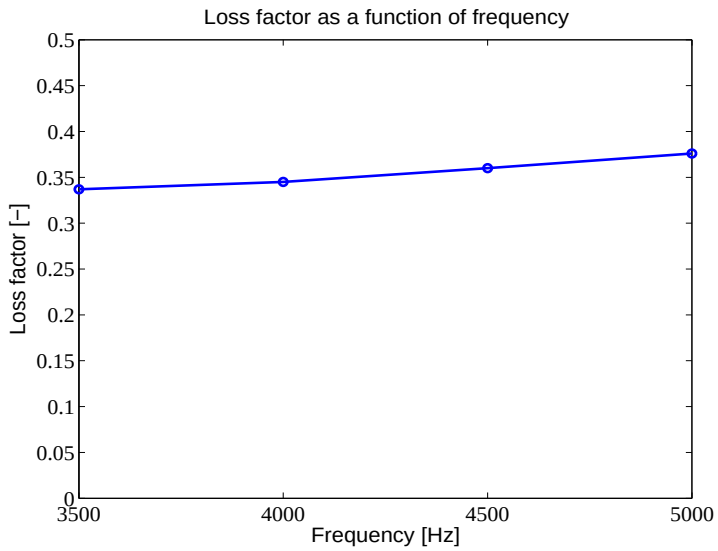

Figure 5.6: *Figure depicts loss factor as a function of frequency.*

5.2 Scatter

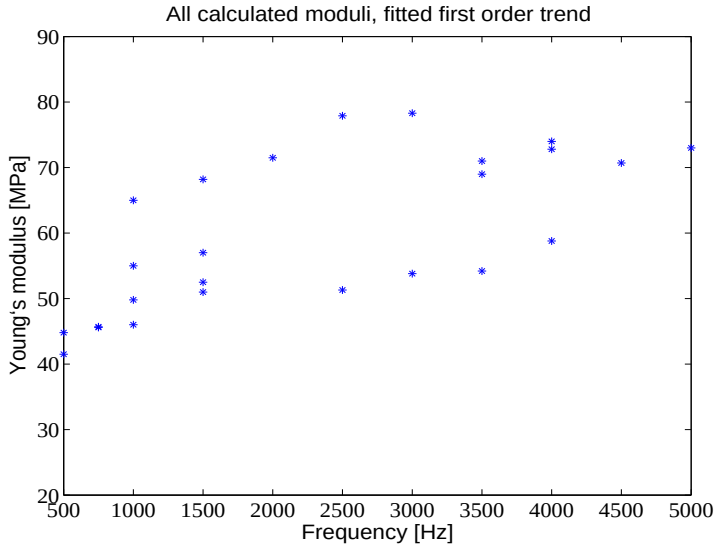

Figure 5.7: *Figure depicts a scatter plot of all estimated Young's moduli.*

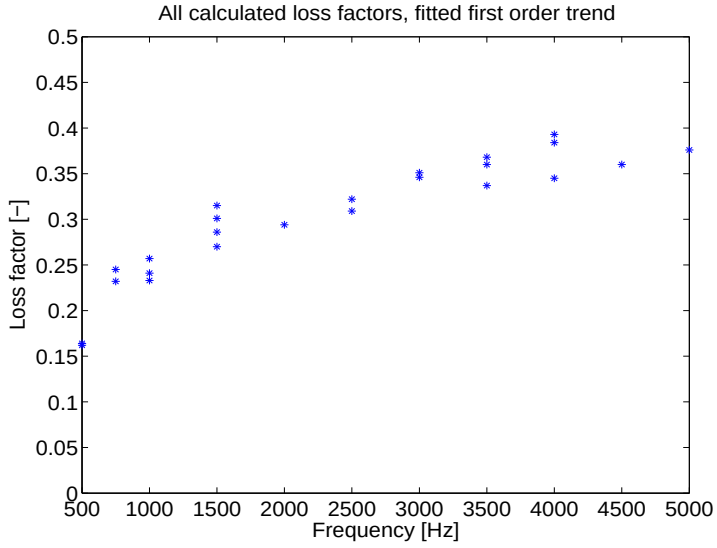

Figure 5.8: *Figure depicts a scatter plot of all estimated loss factors.*

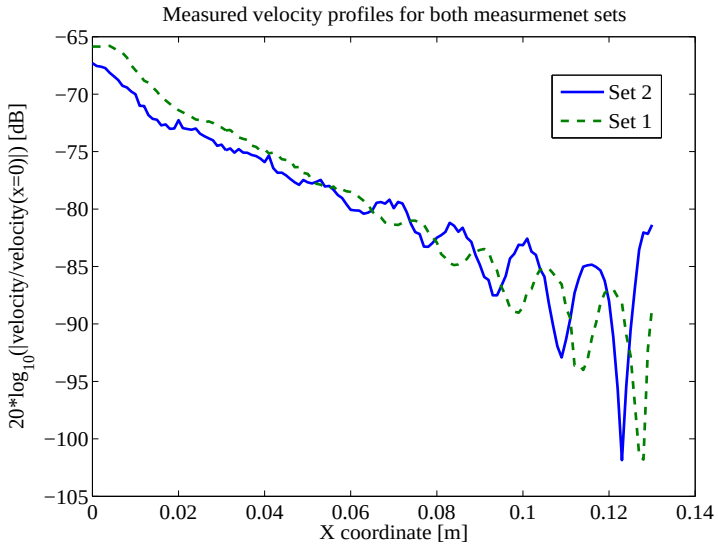

Figure 5.9: *Figure depicts the velocity profiles for sample B at 2500 Hz for both measurement sets*

5.3 Discussion

Based on the results from the independent measurement sets and different samples it seems as if the loss factor is decided with greater accuracy than the Young's modulus. The loss factor increases consistently with frequency while the Young's modulus fluctuates some. Judging from literature (e.g. see Figure 2.4) it seems more logical that the material parameters wold show a gradually increasing behavior within the investigated frequency range.

Notice the overlap, where both samples are tested at the same frequency for measurement set one, in Figure 5.1 and Figure 5.2. The values of the material parameters do not differ more than approximately 10%, i.e. within the limits of what was aimed at. This is not true for the overlaps in Figure 5.3 and Figure 5.4, depicting the second measurement set. Here the Young's modulus values differ by around 30%, while the Loss factor values still lie within a 10% interval. Comparing the two independent measurement sets show an interesting fact. The calculated material parameters for sample A do not differ significantly between the two measurements sets, though for sample B they do. For sample B the Young's modulus values differ between 20-30%, while the Loss factor values again show relatively low difference between the measurement sets. The large difference in estimated Young's modulus is a results of the velocity profile difference between the measurement sets (see Figure 5.9). Wether this is due to accuracy in the measurement process or slight dissimilarity between the samples is difficult to argue. One problem might be the

effect of torsional motion if what is assumed to be the centerline of the sample does not coincide with the neutral axis of torsion.

The overlap of frequencies (i.e. 3500 and 4000 Hz) between measurement set one and two, and for the reduced sample C also shows interesting results. While the error between measurement set two and reduced sample C are small (< 5%) they both disagree with measurement set one.
Figure 5.7, showing all the calculated Young's moduli in a scatter plot, shows an interesting trend. The modulus seems to increase with frequency but they might be a bit to spread out to draw any final conclusions in the matter. It would be in great interest to test a bigger set of rubber samples to see if the calculated moduli follows any statistical distribution.

Figure 5.8, which depicts the scatter of calculated loss factors, shows a very distinct trend. The loss factor value seems to have a clear increasing behavior over frequency. Again is there not sufficiently many independent measurements to draw any type of statistical conclusions.

Except for the discrepancy between the velocity profiles of measurement set one and two there are other factors that might influence the results. Insufficient discretisation in the finite-element model might cause an underestimation of the rotational motion occurring at the boundary. This could result in the optimasation algorithm focuses on the parts close to the excitation, due to the higher levels there. Thereby disregarding the wave patter close to the free end of the beam where the levels are lower. The loss factor is not as greatly influenced by the boundary rotation as the Young's modulus.

Chapter 6

Conclusions

The velocity profile matching method as described in this thesis is a relatively reliable method of determining dynamic stiffness and damping in rubber compounds. The method is based on a velocity profile matching between measured and numerically modeled data.

The method has proven to have a number of positive aspects to it. It is a relatively simple method of testing rubber treads. The measurements do not require any equipment that cannot be found in a standard vibrational acoustics laboratory. Although the method of sample cutting presented in this thesis might not be possible to conduct in such a laboratory. The calculations can be done on a standard computer that has access to any computational- and finite-element software. Depending on the frequency range, and thereby element size, of interest though the computational cost has to correspond to the capacity of the computer.

Another positive aspect about the method is that the rubber sample does not have to be cut according to exact, predefined dimensions or shape. The geometry of the rubber sample used for the measurements can just be prescribed when the finite-element model is defined. Although beam shaped samples, as used i n this thesis, are very convenient they are not required. This implies that preexisting samples, originally not intended for testing, can be investigated by the velocity profile matching method.

Maybe the most interesting aspect of the proposed method is that it, unlike many other testing methods, does not evaluate the sample at resonance frequencies. This means that the method is not as limited in frequency. The velocity profile matching method does not seize do work when clear resonance frequencies no longer can be distinguished. It also means that the sample only has to be measured at those frequencies that is of interest for the particular situation.

The different optimisation algorithms used show different advantages in different situations. The grid search is a good method for narrowing down the possible range of the parameter values and if repeating the process several times and each time making the grid narrower yields convergence. However the accuracy and

stability of the descent algorithms are in some cases greater. The biggest advantage with the grid search algorithm is the simplicity in using it. The only required input is an upper and a lower limit of parameter values and the resolution of the grid. The descent algorithms, as implemented here, require some tuning with the step sizes before working satisfactory. Despite this the accuracy and stability of the descent algorithms cause them be being used exclusively for the results presented.

Future work would be to try improve the repeatability of the measurements. To investigate the sensitivity of the measurement process it could be of interest to dismount and remount the setup between two measurements. Or maybe to change some parameters, such as amplitude, between measurements on the same sample.

Appendix A
FEM applied to structural mechanics

The finite-element method is a very widely used method within a number of fields of engineering. Considering our case which is a structural mechanical problem the mathematical approach of putting up the equations, breaking them down to finite element equations and finally solving them will be explained in this section. it will start with the kinematic relations and via the constitutive relations end up with the equilibrium relations. This equation will then be broken down to a final approximate solution with the help of finite element technique.

Under the assumption of small strains ($(\frac{\partial u_x}{\partial x})^2 \ll 1$) it can be deduced that the normal strains are equal to the respective first derivative of the displacement field while the shear strain is the derivatives, with respect to the plane of the shear, of the same displacement field. This means that the quadratic terms in the Lagrange-Green strain tensor is neglected. These strains are sometimes referred to as engineering strains and are collected in the so called Voight matrix representation according to (A.1)

$$\boldsymbol{\varepsilon} = \tilde{\nabla}\mathbf{u} \tag{A.1}$$

Here $\boldsymbol{\varepsilon}$ represents the strain vector while $\tilde{\nabla}$ is a matrix differential operator and $\mathbf{u}$ is the displacement field.

$$\boldsymbol{\varepsilon} = \begin{pmatrix} \varepsilon_x \\ \varepsilon_y \\ \varepsilon_z \\ \gamma_{xy} \\ \gamma_{yz} \\ \gamma_{xz} \end{pmatrix}, \tilde{\nabla} = \begin{pmatrix} \frac{\partial}{\partial x} & 0 & 0 \\ 0 & \frac{\partial}{\partial y} & 0 \\ 0 & 0 & \frac{\partial}{\partial z} \\ \frac{\partial}{\partial y} & \frac{\partial}{\partial x} & 0 \\ \frac{\partial}{\partial z} & 0 & \frac{\partial}{\partial x} \\ 0 & \frac{\partial}{\partial z} & \frac{\partial}{\partial y} \end{pmatrix}, \mathbf{u} = \begin{pmatrix} u_x(\mathbf{x},t) \\ u_y(\mathbf{x},t) \\ u_z(\mathbf{x},t) \end{pmatrix}.$$

Since small strains are considered it is assumed that the material has a linear response. Thus the constitutive relation we use is Hooke's generalized law (A.2) or Cauchy elasticity,

$$\boldsymbol{\sigma} = \mathbf{D}\boldsymbol{\varepsilon}, \tag{A.2}$$

where $\boldsymbol{\sigma}$ represents the stress field and $\mathbf{D}$ the constitutive matrix. The constitutive relation is assumed to be hyperelastic, meaning that the strain energy is not dependent of how the strain state was obtained but only the sate itself.

$$\sigma = \begin{pmatrix} \sigma_x \\ \sigma_y \\ \sigma_z \\ \tau_{xy} \\ \tau_{yz} \\ \tau_{xz} \end{pmatrix}, \mathbf{D} = \frac{1}{E} \begin{pmatrix} 1 & -\nu & -\nu & 0 & 0 & 0 \\ -\nu & 1 & -\nu & 0 & 0 & 0 \\ -\nu & -\nu & 1 & 0 & 0 & 0 \\ 0 & 0 & 0 & 2(1+\nu) & 0 & 0 \\ 0 & 0 & 0 & 0 & 2(1+\nu) & 0 \\ 0 & 0 & 0 & 0 & 0 & 2(1+\nu) \end{pmatrix}$$

Here E is the Young's modulus and ν is the Poisson's ratio, which is the ratio of transverse contraction strain to longitudinal extension strain in the direction of stretching force. Now consider the equilibrium relations. More precisely dynamic equilibrium which states that the force acting on a body is equal to the inertia force. This might be more familiar as Newton's second law. If we also assume that our structure experiences viscous behavior, which ought to be correct since we previously stated that our tread material is considered to have viscoleastic properties, damping can be added in the equilibrium equation as being proportional to the displacement rate (velocity). This yields,

$$\tilde{\nabla}^T \boldsymbol{\sigma} + \mathbf{U} + c\dot{\mathbf{u}} = \rho\ddot{\mathbf{u}}. \tag{A.3}$$

Where $\mathbf{U}$ is a volume force field acting on the body, c is the viscous damping factor, ρ is the density of the body and $\tilde{\nabla}^T$ is a matrix differential operator. Now the combination of the kinematic, constitutive and equilibrium relations give,

$$\rho\ddot{\mathbf{u}} + c\dot{\mathbf{u}} - \tilde{\nabla}^T \mathbf{D} \tilde{\nabla} \mathbf{u} = \mathbf{U}. \tag{A.4}$$

If harmonic excitation is considered the displacement can be expressed as an amplitude times a phase as,

$$\mathbf{u} = \hat{\mathbf{u}} e^{j\omega t}. \tag{A.5}$$

Where j denotes imaginary number ($\sqrt{-1}$) and ω the angular frequency ($2\pi f$). If the conditions are considered as time invariant. This together with stating that manipulations are done in the frequency domain gives a simple derivation (with respect to time) of the displacement term. Since it is known that the first and the second time derivative of the displacement gives velocity respectively acceleration this gives the simple relations,

$$\mathbf{v} = \dot{\mathbf{u}} = \hat{\mathbf{u}} e^{j\omega t} = j\omega \hat{\mathbf{u}} e^{j\omega t} = j\omega \mathbf{u} \tag{A.6}$$

and,

$$\mathbf{a} = \dot{\mathbf{v}} = \ddot{\mathbf{u}} = \hat{\mathbf{v}} e^{j\omega t} = j\omega \hat{\mathbf{v}} e^{j\omega t} = j\omega \mathbf{v} = -\omega^2 \mathbf{u}. \tag{A.7}$$

Where $\mathbf{v}$ denotes velocity and $\mathbf{a}$ acceleration. Now it is possible to write the equilibrium equation as a function of only the displacement field variable $\mathbf{u}$,

$$(-\omega^2 \rho + cj\omega + \mathbf{K})\mathbf{u} = \mathbf{U}. \tag{A.8}$$

Where K replaces the expression $\tilde{\nabla}^T\mathbf{D}\tilde{\nabla}$. This formulation of the equilibrium equation is commonly referred to as the "strong" formulation. However this equation is in most cases not possible to solve analytically. Therefore the weak form is introduced. What is done mathematically is that the equilibrium equation is multiplied by an arbitrary weight function (v) and integrate over the relevant region. This yields,

$$\int_\Omega v[(-\omega^2\rho d\mathbf{\Omega} + cj\omega + \mathbf{K})\mathbf{u} - \mathbf{U}] = 0 \tag{A.9}$$

Where Ω is the domain (region) of interest. This equation can be separated into,

$$-\int_\Omega v\omega^2\rho\mathbf{u}d\mathbf{\Omega} + \int_\Omega vcj\omega\mathbf{u}d\mathbf{\Omega} + \int_\Omega v\mathbf{K}\mathbf{u}d\mathbf{\Omega} = \int_\Omega v\mathbf{U}d\mathbf{\Omega}. \tag{A.10}$$

The solution for the elements in the variable $\mathbf{u}$ is approximated as

$$u^{app} = \boldsymbol{\psi}\boldsymbol{a} \tag{A.11}$$

Where $\mathbf{a}$ is a vector of unknown parameters ($[a_1\ a_2\ \dots\ a_n]^T$) and $\boldsymbol{\psi}$ is a vector of trial(basis) functions ($[\psi_1\ \psi_2\ \dots\ \psi_n]$) depending on the spatial dimensions over which you integrate (normally x,y,z). Replacing $\mathbf{u}$ with $\mathbf{u}^{\mathrm{app}}$ (which is a vector containing u^{app} for all spatial dimensions) in equation A.10 yields a numerical solution for the equilibrium equation which compared to the analytical solution gives an error $\mathbf{e}$. This error is commonly referred to as the residual (Ottosen and Petersson 1992). The residual depends on the parameters in $\mathbf{a}$. To minimize the residual (error) the weight functions $\mathbf{v}$ ought to be chosen so that $\mathbf{ve}$=0. This minimization can be done with several different methods, e.g. "Point collocation method", "Least-squares method" or "Galerkin's method" mentioned in Ottosen and Petersson (1992). Dealing with finite element techniques Galerkin's method is a very common and powerful method (Ottosen and Petersson 1992). Galerkin's method says that the weight functions should be chosen so that they are equal to the trial/base function. This implies that the trial/base functions are orthogonal to the residual (v^Te=0). Dividing the problem into finite elements and choosing the weight functions according to Galerkin will yield four matrices, one matrix containing the load at each node which will be referred as $\mathbf{R}$, one matrix containing the stiffness of each element ($\mathbf{K}$), one containing the mass of each element ($\mathbf{M}$) and one containing the damping of each element ($\mathbf{C}$). These matrices are defined as

$$\mathbf{M} = \int_\Omega \rho d\mathbf{\Omega} \tag{A.12}$$

$$\mathbf{K} = \int_\Omega \tilde{\nabla}^T\mathbf{D}\tilde{\nabla}d\mathbf{\Omega} \tag{A.13}$$

$$\mathbf{C} = \int_\Omega cd\mathbf{\Omega} \tag{A.14}$$

$$\mathbf{R} = \int_{\Omega} \mathbf{U} d\mathbf{\Omega} \tag{A.15}$$

This leads to the final formulation of our problem in the meaning of a finite element solution. Equation A.16 shows this formulation.

$$(-\omega^2 \mathbf{M} + j\omega \mathbf{C} + \mathbf{K})\mathbf{u} = \mathbf{R} \tag{A.16}$$

Appendix B

Theory of Laser Doppler Vibrometer (LDV)

B.1 Fundamental physics of the LDV

The laser Doppler vibrometer used for the measurement setup described in this thesis is a Helium Neon laser. This means that the medium inside the laser is a gas mixture a Helium and Neon. The LDV measures the normal displacement of the object it is set on. This works as following, an output excitation (or an outside source) causes a certain object to vibrate. The LDV sends out a laser beam which reflects of the vibrating object. The backscattered light interferes with a references beam inside the scanning head and the interference pattern is recorded by a photo detector (see Figure B.1). A voltage level proportional to the vibration velocity is sent out by the vibrometer. The voltage is then digitalized and processed in he software.

This is based on the so called Doppler effect. The Doppler effect is the phenom-

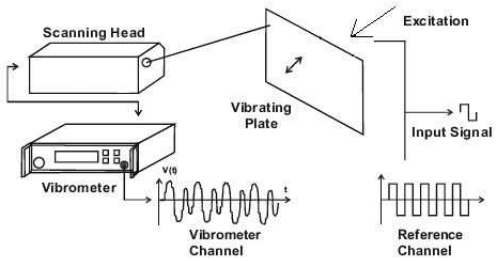

Figure B.1: *A schematic explanation of the data acquisition of the LDV.*

ena that occurs when an object that is radiating waves, is in motion. This causes a shift in wavelength compared to a object that would be still or move in another direction. Thus, is the vibrating object is moving towards the origin of the laser the backscattered light will have shorter wave length than the reference signal. Analogous, is the vibrating object is moving away from the laser source the light has a longer wave length than the reference signal. The interference pattern between the backscattered light and the reference signal provides information of the magnitude of the vibration but not the phase. The phase information comes from frequency modulating the reference signal so that when the amplitude of the vibrating object is zero forward and backward direction is already defined.

B.2 Averaging

The LDV gives a complex number in each scanning point in the frequency domain. The recorded time signal is Fourirer transformed, and an average of all the recordings is made. This means that the measurements are performed several times (depending on the settings) in the same point and than averaged. This is done in order to reduce the influence of noise in the measurement data. Since noise is commonly of random nature, a sufficient number of averages will make the interference due to noise is negligible. If $\underline{C_i}$ denotes a complex number, in the frequency domain, then the frequency domain averaging is done according to:

$$avr(\underline{C}) = \frac{\sum_{i=1}^{N} \Re[\underline{C_i}] + i * \sum_{i=1}^{N} \Im[\underline{C_i}]}{N} \tag{B.1}$$

where N is the number of averages chosen in the settings.

Appendix C
Velocity profiles

C.1 Sample set: 1

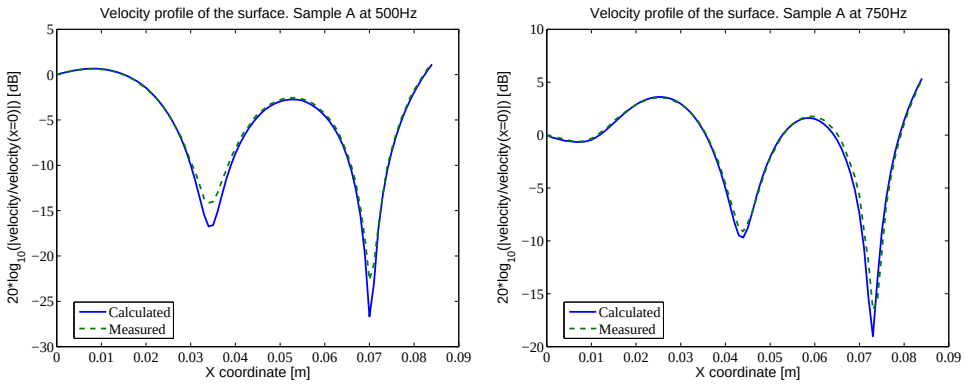

(a) (b)

Figure C.1: *(a) Figure depicts the velocity profiles for sample A at 500hz. (b) Figure depicts the velocity profiles for sample A at 750hz.*

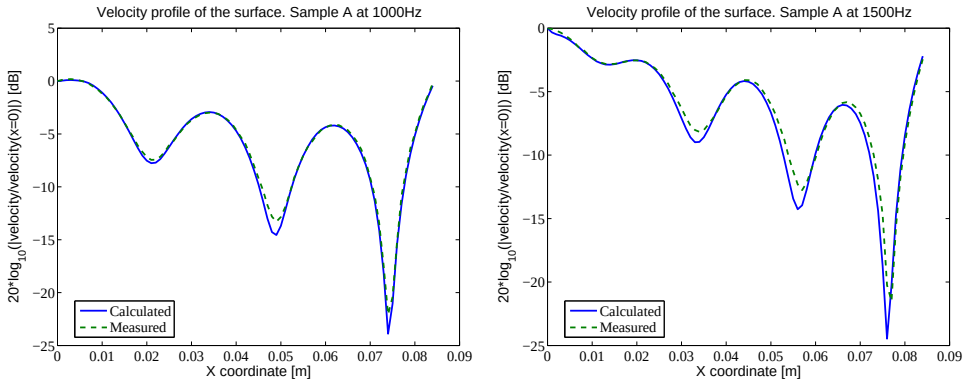

(a) (b)

Figure C.2: *(a) Figure depicts the velocity profiles for sample A at 1000hz. (b) Figure depicts the velocity profiles for sample A at 1500hz.*

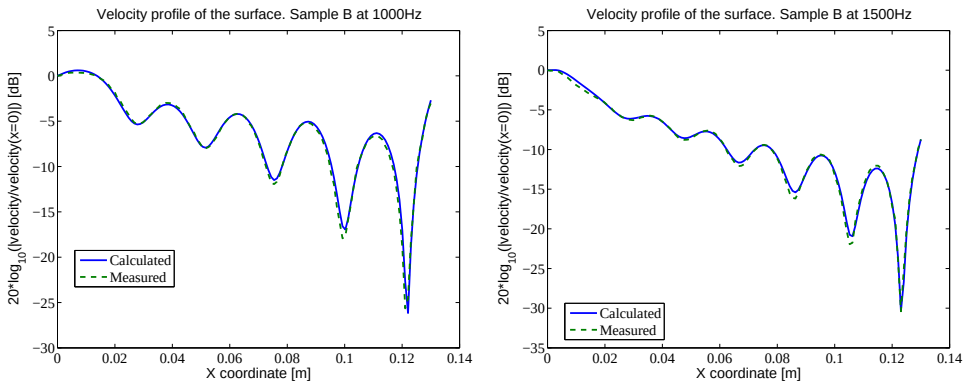

(a) (b)

Figure C.3: *(a) Figure depicts the velocity profiles for sample B at 1000hz. (b) Figure depicts the velocity profiles for sample B at 1500hz.*

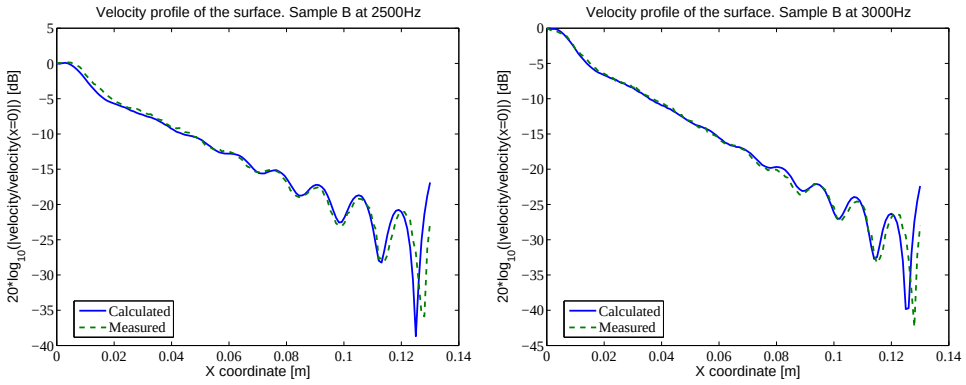

(a) (b)

Figure C.4: *(a) Figure depicts the velocity profiles for sample B at 2500hz. (b) Figure depicts the velocity profiles for sample B at 3000hz.*

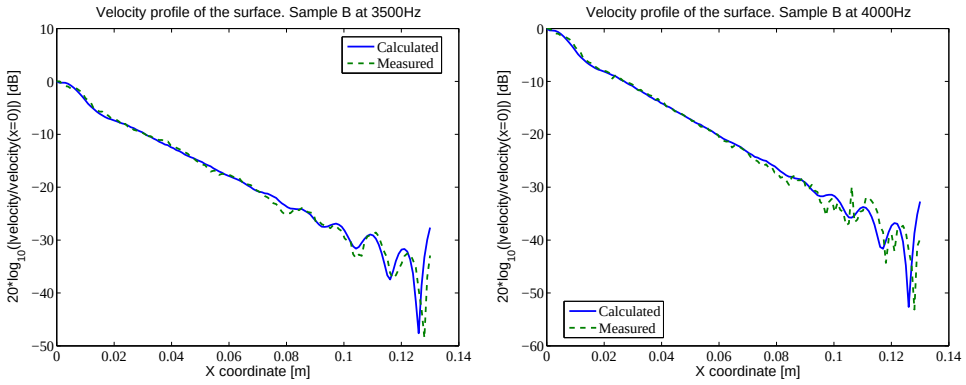

(a) (b)

Figure C.5: *(a) Figure depicts the velocity profiles for sample B at 3500hz. (b) Figure depicts the velocity profiles for sample B at 4000hz.*

C.2 Sample set: 2

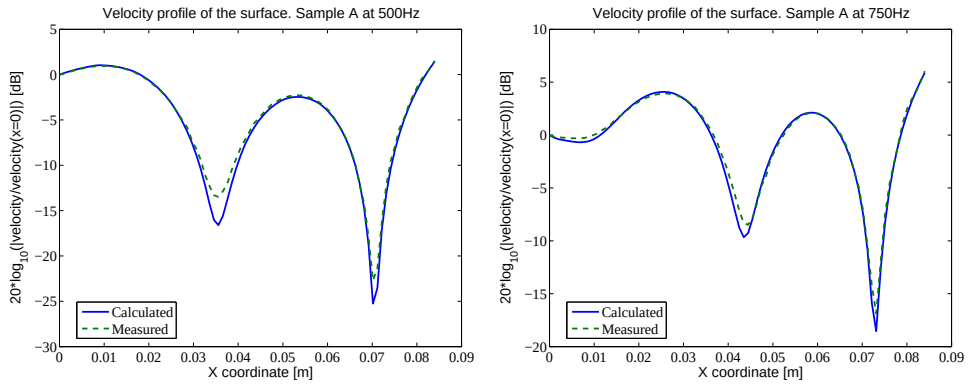

(a) (b)

Figure C.6: *(a) Figure depicts the velocity profiles for sample A at 500hz. (b) Figure depicts the velocity profiles for sample A at 750hz.*

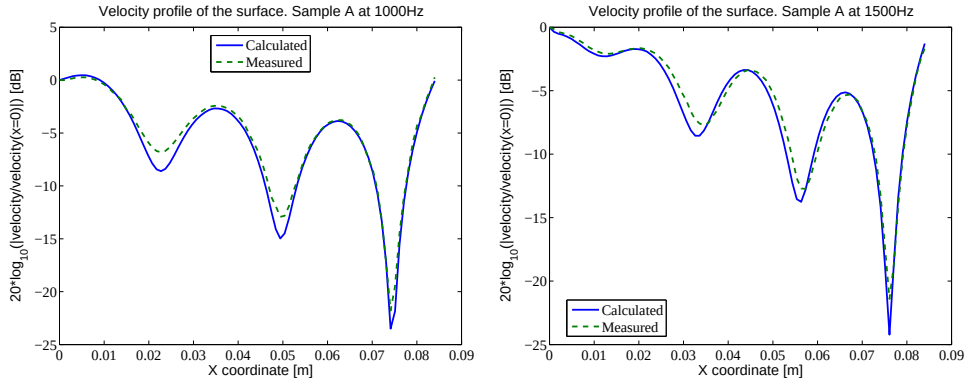

(a) (b)

Figure C.7: *(a) Figure depicts the velocity profiles for sample A at 1000hz. (b) Figure depicts the velocity profiles for sample A at 1500hz.*

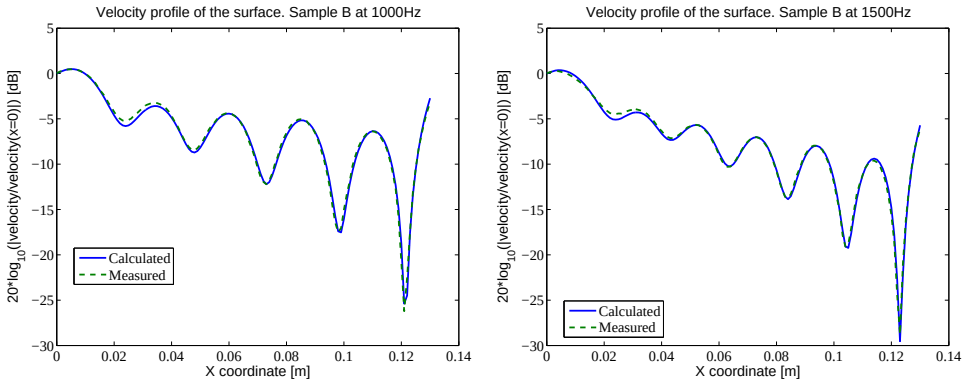

(a) (b)

Figure C.8: *(a) Figure depicts the velocity profiles for sample B at 1000hz. (b) Figure depicts the velocity profiles for sample B at 1500hz.*

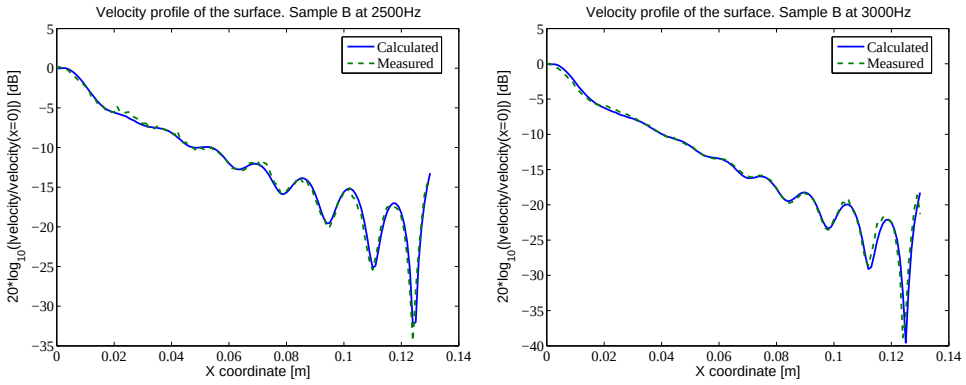

(a) (b)

Figure C.9: *(a) Figure depicts the velocity profiles for sample B at 2500hz. (b) Figure depicts the velocity profiles for sample B at 3000hz.*

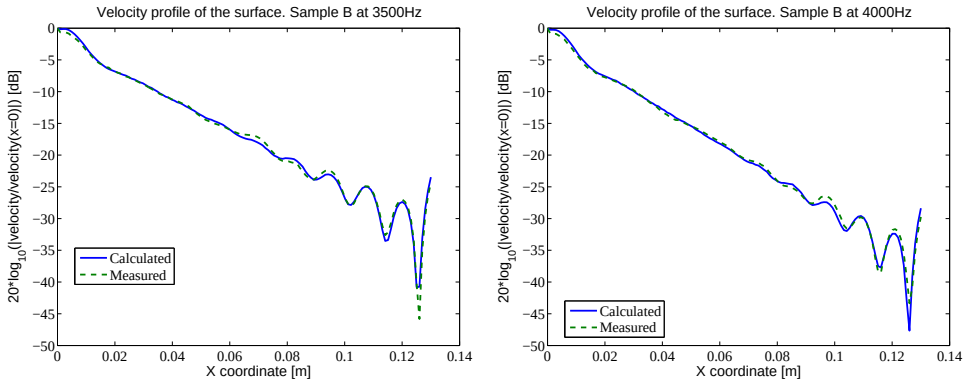

(a) (b)

Figure C.10: *(a) Figure depicts the velocity profiles for sample B at 3500hz. (b) Figure depicts the velocity profiles for sample B at 4000hz.*

C.3 Sample set: reduced sample C

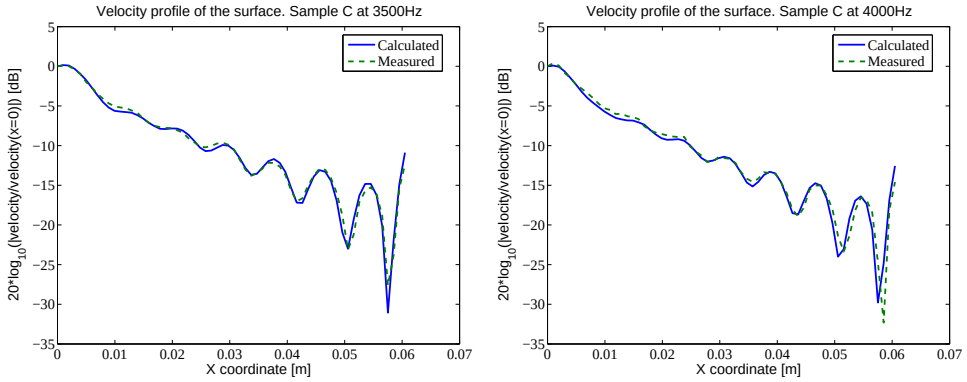

(a) (b)

Figure C.11: *(a) Figure depicts the velocity profiles for shortened sample C at 3500hz. (b) Figure depicts the velocity profiles for shortened sample C at 4000hz.*

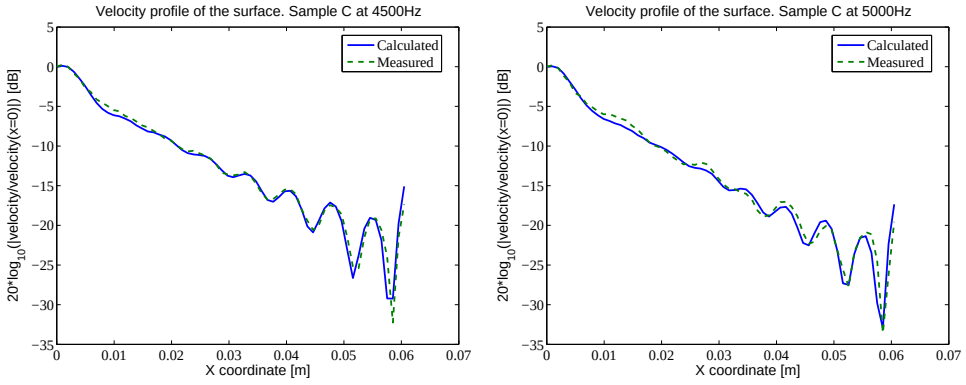

(a) (b)

Figure C.12: *(a) Figure depicts the velocity profiles for shortened sample C at 4500hz. (b) Figure depicts the velocity profiles for shortened sample C at 5000hz.*

Appendix D
Measurement equipment

The following equipment were used for the measurements conducted in this thesis:
Shaker; B& K Type 4810
Force transducer; B& K Type 8203
Signal amplifier; NAD SA 3020
Charge amplifier; B& K Type 2635
LDV; PSV 300
Temperature probe; Labfacility model 2020L

References

P. Andersson. Modelling interfacial details in tyre/road contact - adhesion forces and non-linear contact stiffness, 2005.

P. Andersson. Estimation of tread properties. unpublished.

R. Brown. *Handbook of polymer testing*. Marcel Dekker, Inc., 1999.

M. Coja. Effective vibro-acoustical modelling of rubber isolators., 2005.

L. Cremer and M. Heckl. *Structure born sound*. Springer-Verlag, 1987.

J.P. Dussault. Convergence of implementable descent algorithms for unconstrained optimization. *J.O.T.A*, 2000.

M.T. Heath. *Scientific computing*. McGraw-Hill, 2002.

ISO 23529:2004. Rubber-general procedures for preparing and conditioning test pieces for physical test methods.

ISO 4664-1:2005. Rubber, vulcanized or thermoplastic - determination of dynamical properties - part 1: General guidance.

D.I.G. Jones. *Handbook of viscoelastic vibration damping*. Wiley, 2001.

J.E. Mark, B. Erman, and F.R. Eirich. *Science and technology of rubber*. Academic Press, 1994.

N. Ottosen and H. Petersson. *Introduction to the finite element method*. Prentice Hall, 1992.

E. Polak. *Optimization- algorithms and consistent approximations*. Springer-Verlag, 1917.

L. Yuan and Om. P Agrawal. A numerical scheme for dynamic systems containing fractional derivatives. *ASME, Design Engineering Technical Conferences*, 1998.